Energy and Cost Assessment of Adaptive Structures: Case Studies

Gennaro Senatore, Dr.Eng.[1]; Philippe Duffour, Ph.D.[2]; and Pete Winslow, Ph.D.[3]

Abstract: This paper demonstrates how adaptive design (details published elsewhere) can be employed to save, on average, 70% of whole-life energy on a range of spatial structures, the whole-life energy deriving from an embodied part in the material and an operational part for structural adaptation. Assuming some statistical distribution for the probability of occurrence of the loads, whole-life energy is minimized by combining optimal material distribution and strategic integration of the actuation system, which is only used when loading events exceed a certain threshold. Instead of using more material to cope with the effect of the loads, the active elements change the shape of the structure in order to homogenize the stresses and keep deflections within limits. Five case studies are investigated here: a tall building core, a trussed portal frame, a long-span arch bridge, a 3-pin roof arch, a double-curved shell, and an office tower supported by an exoskeleton structural system. The purpose of the case studies described in this paper is to study (1) adaptive structure performance in terms of mass and energy savings as well as monetary costs for both strength- and stiffness-governed design problems; and (2) design scalability to complex spatial configurations. The case studies confirmed that even for large complex structures, significant energy savings can be achieved, the more so as the structure becomes more stiffness-governed. In this case, the adaptive solution becomes competitive also in terms of monetary costs.
DOI: 10.1061/(ASCE)ST.1943-541X.0002075. *This work is made available under the terms of the Creative Commons Attribution 4.0 International license, http://creativecommons.org/licenses/by/4.0/.*

Author keywords: Adaptive structures; Active structural control; Shape control; Load path optimization; Whole-life energy; Structural optimization.

Downloaded from ascelibrary.org by University College London on 06/20/18. Copyright ASCE. For personal use only; all rights reserved.

Introduction

Adaptation in Structural Applications

Adaptive structures are defined here as structures capable of actively counteracting the effect of external loads via controlled shape changes and redirection of internal load paths. These structures are integrated with sensors (e.g., strain, vision), control intelligence, and actuators. In civil engineering, active control has focused mostly on the control of vibrations for building or bridges to improve safety and serviceability during exceptionally high loads such as strong winds and earthquakes) (Soong and Chang 1982; Soong 1988). Active brace systems have been tested using hydraulic actuators fitted as cross-bracing elements of the structure, directly controlling its deflections using actively controlled forces (Abdel-Rohman and Leipholz 1983; Reinhorn et al. 1992). Displacement control in cable-stayed bridges can be obtained via control forces provided by the stay cables working as active tendons (Rodellar et al. 2002; Xu et al. 2003). Active cable tendons can also be used to change the amount of prestress in reinforced concrete beams and in steel trusses to limit displacements under loading (Schnellenbach and Steiner 2014). Integration of actuators has been shown to be an effective way to suppress vibrations in truss structures with high stiffness-to-weight ratios (Preumont et al. 2008).

Active structural control has also been used in applications for shape control. Some all-weather stadia use deployable systems for expandable/retractable roofs. These include, for example, the Singapore National Stadium (Henry et al. 2016) and the Wimbledon Centre Court (SCX 2010). Active tensegrity structures—structures whose stability depends on self-stress—have been used as deployable systems in aerospace (Tibert 2002) and investigated for displacement control (e.g., Fest et al. 2003; Adam and Smith 2008). Active compliant structures, which can be thought of as structures working as monolithic mechanisms (Campanile 2005; Hasse and Campanile 2009), have been studied for deployment of antenna reflectors and shape control of aircraft wings to improve maneuverability (Jenkins 2005).

Actuation has been used to modify the membrane stress state in thin plates and shells when disturbances such as local loadings, cuttings, or residual stress occur after formworks removal (Sobek 1987). In these cases, because the load-carrying capacity is significantly reduced, actuation in the form of induced strain or support displacement (actively controlled bearings) can be used to homogenize the stress field and, in so doing, minimize the maximum stress governing the design (Weilandt 2007; Neuhäuser 2014).

Because of uncertainties in the long-term reliability of sensor and actuator technologies combined with building long service lives and load long return periods, the recent trend has been to develop active structural control to meet serviceability requirements rather than to contribute to strength/safety improvement (Korkmaz 2011). In this context, adaptive structures offer an emerging design paradigm that deals with providing stiffness in a completely different way from that in traditional engineering. Although the strength

[1]Applied Computing and Mechanics Laboratory (IMAC), Swiss Federal Institute of Technology (EPFL), School of Architecture, Civil and Environmental Engineering (ENAC), Station 18, CH-1015 Lausanne, Switzerland (corresponding author). ORCID: https://orcid.org/0000-0001-7418-9713. Email: gennaro.senatore@epfl.ch

[2]Dept. of Civil Environmental and Geomatic Engineering, Univ. College London, Gower St., WC1E 6BT London, UK.

[3]Expedition Engineering, 4 Maguire St., SE1 2NQ London, UK.

Note. This manuscript was submitted on January 31, 2017; approved on January 8, 2018; published online on May 29, 2018. Discussion period open until October 29, 2018; separate discussions must be submitted for individual papers. This paper is part of the ***Journal of Structural Engineering***, © ASCE, ISSN 0733-9445.

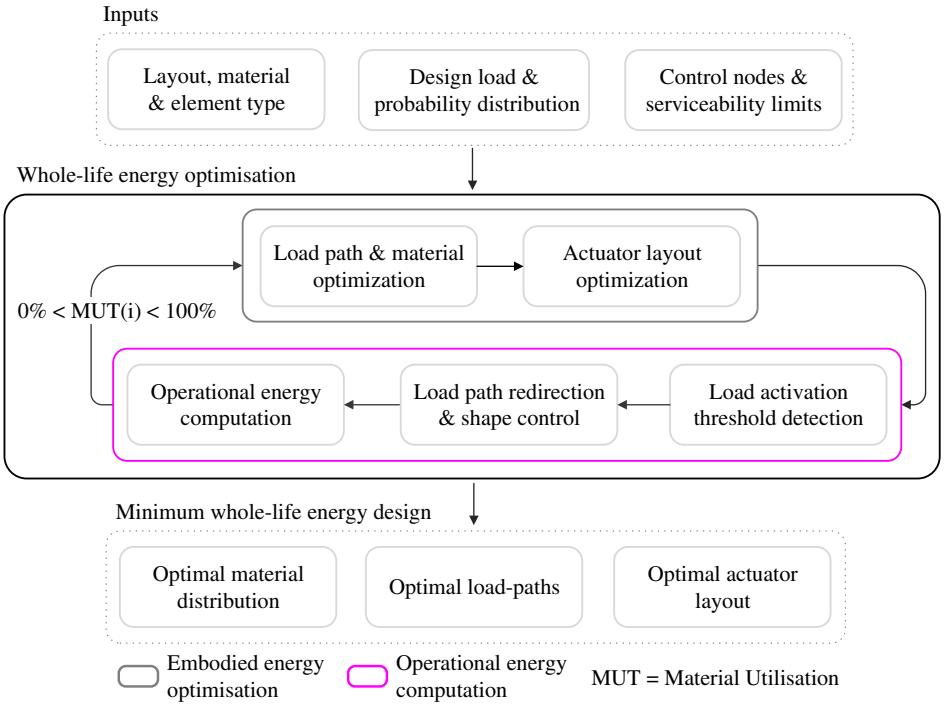

Fig. 1. Design methodology flowchart. [©IOP Publishing. Reproduced with permission. All rights reserved (Senatore et al. 2018).]

of the structure cannot be compromised, trade-offs in the stiffness can be investigated. If the structure relies on an active system for deflection control, its force-displacement response and hence its apparent stiffness can be altered strategically such that the passive-active configuration achieves higher efficiency in terms of whole-life energy.

Adaptive Structure Design Methodology

Most design strategies for adaptive structures aim to minimize a combination of control effort and material mass. Often the structure and the actuation system are designed to be separate, the location of sensors/actuators being decided a priori (Cha et al. 1988; Khot 1998; Soong and Cimellaro 2009). However, a well-chosen actuator layout is critical to minimizing control effort and improving accuracy. The majority of existing methods that address the actuator-placement problem rely on metaheuristics (Lu et al. 1992; Begg and Liu 2000), which give little insight into the mechanics of active force-displacement control. In addition, although the potential of using adaptation to save material mass has been investigated (Onoda and Haftka 1987; Sobek and Teuffel 2001; Teuffel 2004; Utku 1998), whether the energy saved by using less material makes up for the energy consumed through control and actuation is a question that has so far received little attention.

A new optimum design methodology, presented by Senatore et al. (2013), is based on improving structural performance through reduction in the energy embodied in the material at the cost of a small increase in operational energy necessary for structural adaptation. The method is briefly summarized here; the reader is referred to Senatore et al. (2013) for a more detailed presentation. The method has so far been implemented for reticular structures, with which this paper exclusively deals. The process comprises two nested optimization stages as illustrated by the flowchart in Fig. 1.

The outer optimization stage identifies a structure with minimal overall energy (embodied + operational) for a given load distribution. This is done by systematically varying the material utilization factor (MUT), which can be thought of as a scaling factor on the cross sections. Varying the MUT changes the design from a least-weight structure with small embodied but large operational energy to a stiffer structure with large embodied but small operational energy consumption. This is shown diagrammatically in Fig. 2, which describes the notional variation in total energy with the MUT. The inner optimization itself consists of two main optimization steps.

The first step finds the optimum load path and corresponding material distribution, ignoring compatibility and serviceability limit and thus yielding a design that represents a lower bound in terms of material mass. The optimization is subject to equilibrium and ultimate-limit-state constraints including member buckling. The members of the structure are sized so that they have the capacity to meet the worst expected demand from all load cases for strength only. When the structure experiences external loads, the compatible forces in general become different from the optimal forces and the resulting displacements might be beyond serviceability limits. This is addressed by the second step, which finds the optimal actuator layout to actively manipulate the flow of internal forces by

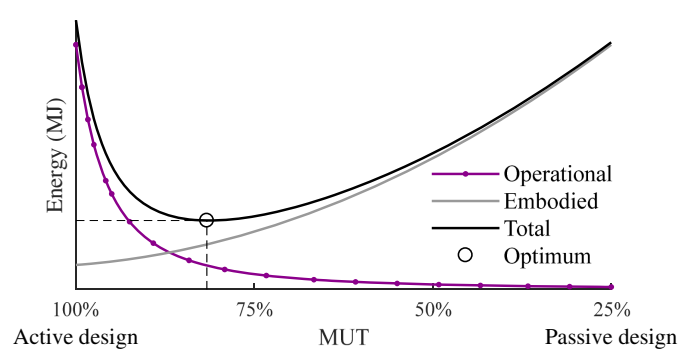

Fig. 2. Embodied, operational, and total energy as a function of MUT. [©IOP Publishing. Reproduced with permission. All rights reserved (Senatore et al. 2018).]

Downloaded from ascelibrary.org by University College London on 06/20/18. Copyright ASCE. For personal use only; all rights reserved.

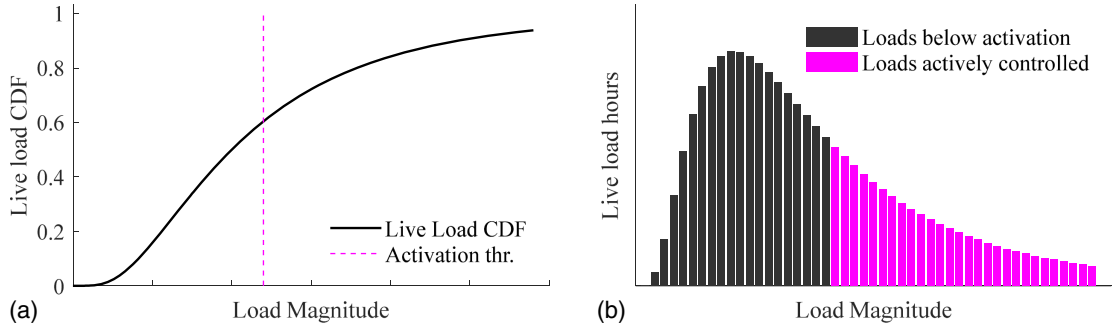

Fig. 3. (a) Live-load cumulative distribution; and (b) live-load hours. [©IOP Publishing. Reproduced with permission. All rights reserved (Senatore et al. 2018).]

Downloaded from ascelibrary.org by University College London on 06/20/18. Copyright ASCE. For personal use only; all rights reserved.

changing the shape of the structure to enforce compatibility and at the same time compensate for displacements. The actuators are thought of as integrated into the structure because they replace some of its members. Once the actuator layout is known, a control strategy is determined. If a change in loads causes a state of stress that violates an ultimate limit state (ULS) or a serviceability limits state (SLS), the load path is redirected and displacements are controlled by the active system. In this way, passive resistance through material and form is replaced by a small amount of operational energy through adaptation.

The structure is designed to take permanent loads as well as randomly fluctuating live loads. The methodology is based on the probability of live loads occurring. In a real design situation, this probability should be based on empirical data or commonly used statistical models for the load considered. For illustrative purposes, a possible example of one such probability distribution function is shown in Figs. 3(a and b). The method identifies the load activation threshold [dashed line in Fig. 3(a)], which is the load level above which actuation is needed for compensation of internal forces and displacements. Fig. 3(b) plots the hours of occurrence for each load level obtained by discretizing the probability density distribution scaled by the total number of hours representing the structure's whole life. The introduction of the load activation threshold shows how passive and active design can be combined to reach a higher level of efficiency. The hybrid passive-active structural system is designed so that in normal loading conditions it takes the load passively while actuators are locked into position. These are used only when the loads reach the activation threshold. In this way, only operational energy is consumed when necessary.

Geometric Exploration

Structural System Selection

Senatore et al. (2013) showed that, with simple planar reticular structures (e.g., simply supported beam truss) designed as just described, substantive savings can be achieved—up to 50% of total energy when compared with identical passive structures designed using state-of-the-art structural optimization methods. The purpose of this paper is to assess the potential of this new design methodology by comparing adaptive design performance against optimized passive performance for a number of hypothetical but realistic structure case studies of increasing complexity. To investigate how the conclusions reached in studying a simple 20-m-span planar truss (Senatore et al. 2013) generalize with scale and complexity, a tall building core, a portal frame, a long-span arch bridge, a 3-pin roof arch, a double-curved trussed shell, and an exoskeleton tower structure (i.e., no cores) are considered. The focus is on challenging structures for which deflection (i.e., stiffness governed) is an issue because actuation and sensor systems are unlikely to be used on more conventional structures. Further justification of structure selection is provided in the description of each case study. In this section, common assumptions and terms of comparison are presented. The results for each case study are presented in the section "Case Studies."

Actuator Type, Dynamics, and Control System Energy Consumption

It is assumed throughout that linear actuators are used with a mechanical efficiency of 80%. For civil engineering structures, the magnitude of the forces to be controlled likely orient the choice toward hydraulic actuators. The mechanical efficiency of hydraulic actuators is 90–98% (Huber et al. 1997). For this reason, the assumption of actuator mechanical efficiency is conservative.

The operational frequency of the actuators is set to the first natural frequency of the structure because this is likely to be the frequency that will dominate the response of most lightly damped structures excited by wind, earthquakes, or pedestrians. This assumption is conservative because it implies that, even for a quasi-static or low-frequency response, the actuators always work at the first natural frequency of the structure. It is assumed that vibration control is dealt with by nonactive means (e.g., tuned mass dampers) if required. Although the active system could be used to compensate for this effect, doing so could result in the expense of significant additional operational energy because vibrations can occur very often.

The energy it takes to power the control system (e.g., sensors and signal processing) is modeled as a linear function of the number of sensors and actuators. This assumption is based on empirical knowledge gained via experimental testing on a purpose-built large-scale adaptive truss prototype (Senatore et al. 2018). The control system energy is part of the total operational energy, but it is not related to the energy needed for structural adaptation (i.e., load path and shape control). The former is usually substantially lower than the latter. The control system energy requirement becomes important for small structures because in such cases it is comparable with the embodied energy savings.

Control System Integration

As shown in Senatore et al. (2013), the optimum actuator positions can be determined by selecting those elements whose length change contributes most efficiently to internal force and displacement correction. This analysis requires as input the selection of

a certain number of controlled degrees of freedom (CDOFs), which is usually dictated by serviceability. The minimum number of actuators n^{ACTs} to exactly compensate for all controlled displacements is equal to the sum of the number of CDOFs and the degree of indeterminacy of the structure ($n^{\mathrm{ACTs}} = n^{\mathrm{CDOFs}} + r$) (Senatore et al. 2013). Intuitively, this is the minimum number of actuators needed to turn the structure into a controlled mechanism. If fewer actuators are used, displacements can still be controlled albeit with lower accuracy.

It is assumed that the structures are fitted with as many strain sensors as necessary to compute the displacement field with reasonable accuracy. Structural layout is one of the most important factors influencing control system complexity. To appreciate how the structural layout and the control system are related, control system density (CSD) is here defined by two terms: the number of sensors and the number of actuators per cubic meter of structure (the volume occupied by the material used by the structure).

Statistical Load Modeling

The structures are designed to take a generic permanent load (e.g., self-weight + cladding) as well as a randomly fluctuating load such as wind, earthquakes, crowd loading, or moving loads (e.g., passing trains). For simplicity, these loads are all considered live loads here. Live-load statistics are modeled using a log-normal probability distribution (Fig. 3), which because it is closely related to the normal probability distribution, is general. Also, it takes only positive real values and provides the desired bias toward the lower values of the random variable.

The live-load magnitudes used in this paper are commensurate with those used by practicing design engineers. The design load (excluding the safety factor), hereafter referred to as the characteristic load, is defined as the 95th percentile of the load probability distribution (Nowak and Collins 2012). For simplicity, the mean of the underlying normal distribution is set to zero. Once the mean and characteristic loads are set, the standard deviation is fully characterized. To calculate the total energy consumed throughout the life of the structure, a design life must be assumed. The structures in all case studies are assumed to have been designed for 50 years.

Comparison: Adaptive versus Passive

Structural Elements, Mass, and Energy

All elements have a cylindrical hollow section. To limit optimization process complexity, thickness is set proportional (10%) to external diameter. Actuator mass is assumed to be a linear function of the required force with a constant 0.1 kg/kN (e.g., an actuator with a push/pull load of 1,000 t weighs 1,000 kg) (ENERPAC 2016).

The energy analysis is carried out using a material energy intensity factor (MEI) to convert material mass into embodied energy. The material used in the simulations described in this paper is steel, in the form of rods obtained from predominantly virgin materials (no recycled content), whose energy intensity is 35 MJ/kg as taken from the *Inventory of Carbon and Energy (ICE)* (Hammond and Jones 2008). To benchmark the adaptive structures, an identical passive structure is designed using an optimization routine described in Senatore et al. (2013) that outperforms the modified fully used design method (Patnaik et al. 1998).

Monetary Cost

A monetary cost analysis is carried out for each case study. The main assumptions made are these:

- Actuation is hydraulic. The cost of a hydraulic actuator is assumed to be linearly proportional to the required force (T. Colin and C. Alister, personal communication, 2017) at a rate of 1.35 \$/kN (e.g., an actuator with a push/pull force of 1,000 t costs \$ 13,580). The cost of the hydraulic system (e.g., pumps, loading manifold assembly) and the driver electronics is estimated at \$7,000/actuator (T. Colin and C. Alister, personal communication, 2017).
- The cost of a strain gauge sensor (full-bridge) is set to \$700/unit including lead wires (Vishay 2015).
- The cost for data acquisition (i.e., monitoring) and processing is set to \$700 per channel: one channel per strain sensor, two channels (position feedback and power output) per actuator.
- The cost of construction material (in this case steel) is set to \$7,000/t (TATA Steel 2012).
- The cost of fabrication for the passive and the adaptive structure is assumed to be identical because both structures require fabrication of an equal number of joints and elements.
- Maintenance for actuators and sensors is assumed to happen once per year requiring a full day to inspect 5 actuators and 10 sensors. The cost of one inspection is estimated at \$700/day.

Although these cost figures originate from experience gained via prototyping and experimental testing (Senatore et al. 2018) as well as personal communication with manufacturers (T. Colin and C. Alister, personal communication, 2017), they are used here only to study monetary cost difference variations between the adaptive and passive structure case studies.

Because adaptive structures can be thought of as energy-saving devices, the monetary cost for saving energy using structural adaptation is compared to the cost of producing energy using other technologies [e.g., photovoltaic systems (PVs)]. Using London as installation location, the average cost of producing energy using PVs is set to 0.13 \$/kWh taken from the *National Renewable Energy Laboratory* calculator (NREL 2012). The adaptive minus passive monetary cost difference divided by the energy difference between the two solutions represents the cost of saving energy using structural adaptation.

Ultimate and Serviceability Limit State

Both passive and adaptive structures are subject to the same load factors and ultimate limit state constraints, including member buckling. Limits on deflection used in the examples described in this paper are those commonly used for the design of civil engineering structures—for instance, span/360 to limit vertical displacements and height/500 to limit total building drift. To make a fair comparison, the displacements are assumed to be caused by live load only. The passive structure is thought of as perfectly precambered under permanent load; hence, material distribution is driven to compensate for the deflection caused by live load only. For the adaptive structure, instead, the actuators completely reduce the displacements caused by the permanent load. In this way, both the passive and adaptive structures are already stressed when the live load is applied.

Scope of Comparative Study

Each case study investigates how a plausible adaptive solution compares with an optimized passive solution. The terms of comparison include total energy and monetary cost.

The chosen structural systems fall into two broad categories: Examples 1 and 2 resist transverse loads by bending/shear; Examples 3–6 resist as least some of the loads through membrane action and acquire significant stiffness from their form; Examples 1–3 can be reduced to planar structures; and Examples 3–6 have a three-dimensional (3D) layout. The focus of the paper is on the quasi-static behavior of the structural systems. In principle

Downloaded from ascelibrary.org by University College London on 06/20/18. Copyright ASCE. For personal use only; all rights reserved.

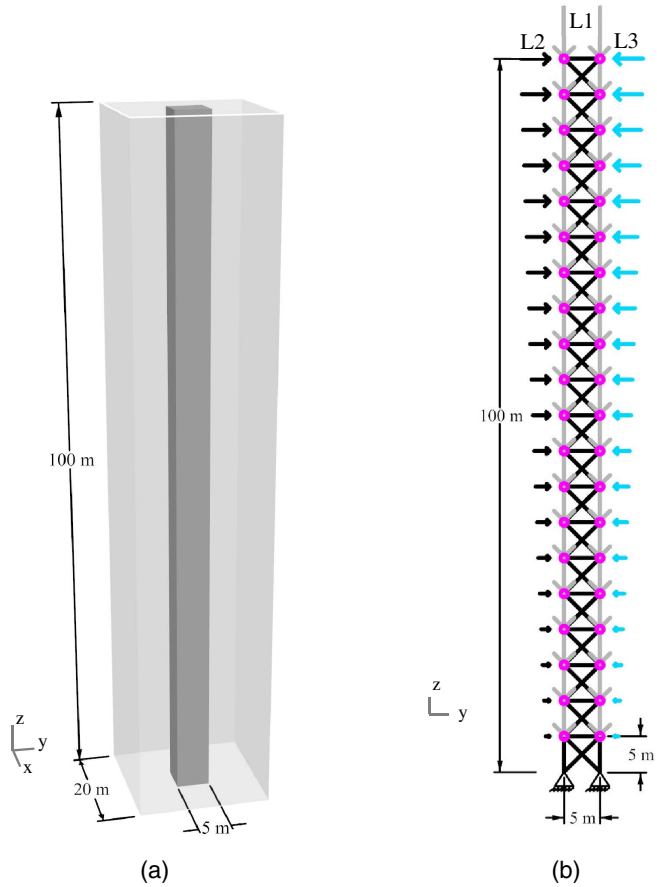

Fig. 4. (a) Multistory building; and (b) loads and controlled nodes (indicated by circles).

seismic hazards can be mitigated using active control. However, this requires dynamics analysis, which is beyond the scope of this investigation.

Because several case studies are investigated, their presentation has been kept relatively short. The results in each case are presented through a series of graphics that are carefully produced to show to scale the key features of the adaptive and passive designs.

Case Studies

Multistory Building Core

The structure considered in this case study is a multistory building core made of four planar vertical trusses as shown in Fig. 4(a). This configuration is investigated because it is deflection-sensitive and ubiquitous; thus, the adaptive solution can help in reducing significantly the environmental impact of this type of load-bearing system. Due to symmetry, the design of the structure can be reduced to that of one of the side planar trusses.

The side planar truss studied supports 20 m of cover out of plane as shown in Fig. 4(a). Fig. 4(b) shows the structural subsystem

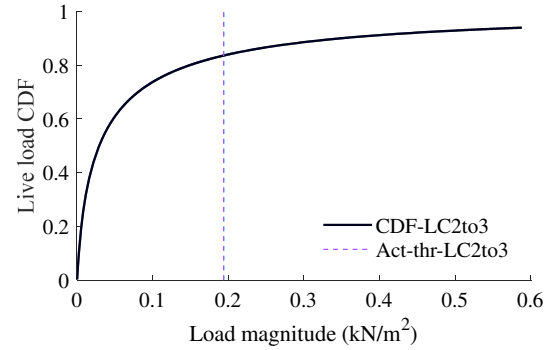

Fig. 5. Live-load CDF and load activation thresholds.

under consideration—a 100-m-tall cantilever truss constrained as indicated in the diagram. Total building drift is limited to height/500 (Griffis 1993). The horizontal displacements of all unconstrained nodes are set as CDOFs for a total of 40 CDOFs. Controlled nodes are indicated by circles in Fig. 4(a). Because the degree of static indeterminacy is 20, the minimum number of actuators to control exactly all selected displacements is 60, as discussed in the section "Control System Integration."

The dead load is set to 3 kN/m^2 resulting in a uniformly distributed load(UDL) of 30 kN/m. Three load cases are considered: one is self-weight + dead load (vertical); the other two are horizontal distributed loads in opposite directions whose intensity varies quadratically, with the height representing a wind-type (live) load. The live-load maximum intensity is set to 0.6 kN/m^2, with a 0.2 ratio of live- to dead-load (L:D), which is equivalent to a wind maximum velocity of 30 m/s (Category-1 hurricane). Table 1 summarizes all load cases.

Fig. 5 shows the live-load cumulative distribution functions (CDFs) for the two cases, LC2 and LC3. The loads have opposite directions but identical probability distributions; therefore, the vertical dashed lines representing the activation thresholds are also identical. In terms of wind velocity, the load activation threshold corresponds to approximately 18 m/s. The total actuation time is 5.2 years (over 50 years), which is approximately 2.6 years for both LC2 and LC3.

Fig. 6(a) shows the embodied, operational, and total energy as the MUT varies. The optimal adaptive configuration is found for a MUT of 45% whereas the passive structure corresponds to a MUT of 17%. This means that the optimized adaptive and passive structures are designed so that the maximum stresses under the worst load combination are 45 and 17% of the yield stress, respectively. Compared with the passive structure, the adaptive structure achieves savings of 63 and 43% in mass and total energy, respectively [Fig. 6(b)].

Fig. 7 compares the optimized passive structure with the adaptive structure. The actuators are represented as integrated in the structure by replacing part of its elements and on the bare layout. The biggest- and smallest-diameter tubes for the adaptive solution are 1,280 and 100 mm for the lowest vertical and horizontal elements, respectively. For the passive solution, these values are more than double. Fig. 7(d) shows the controlled shape after

Table 1. Multistory building core: load combination cases

Case	Load factor	Permanent load	Load factor	Live load
LC1	1.35	L1 = dead load + self-weight	1.5	N/A
LC2 and LC3	1.35	L1 = dead load + self-weight	1.5	L2 and L3 = 1.5 kN/m^2

Downloaded from ascelibrary.org by University College London on 06/20/18. Copyright ASCE. For personal use only; all rights reserved.

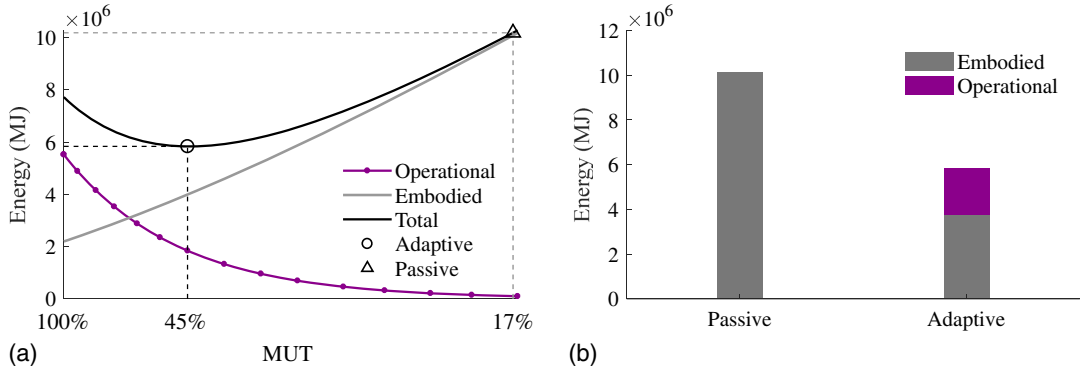

Fig. 6. (a) Embodied, operational, and total energy versus MUT; and (b) passive versus adaptive total energy.

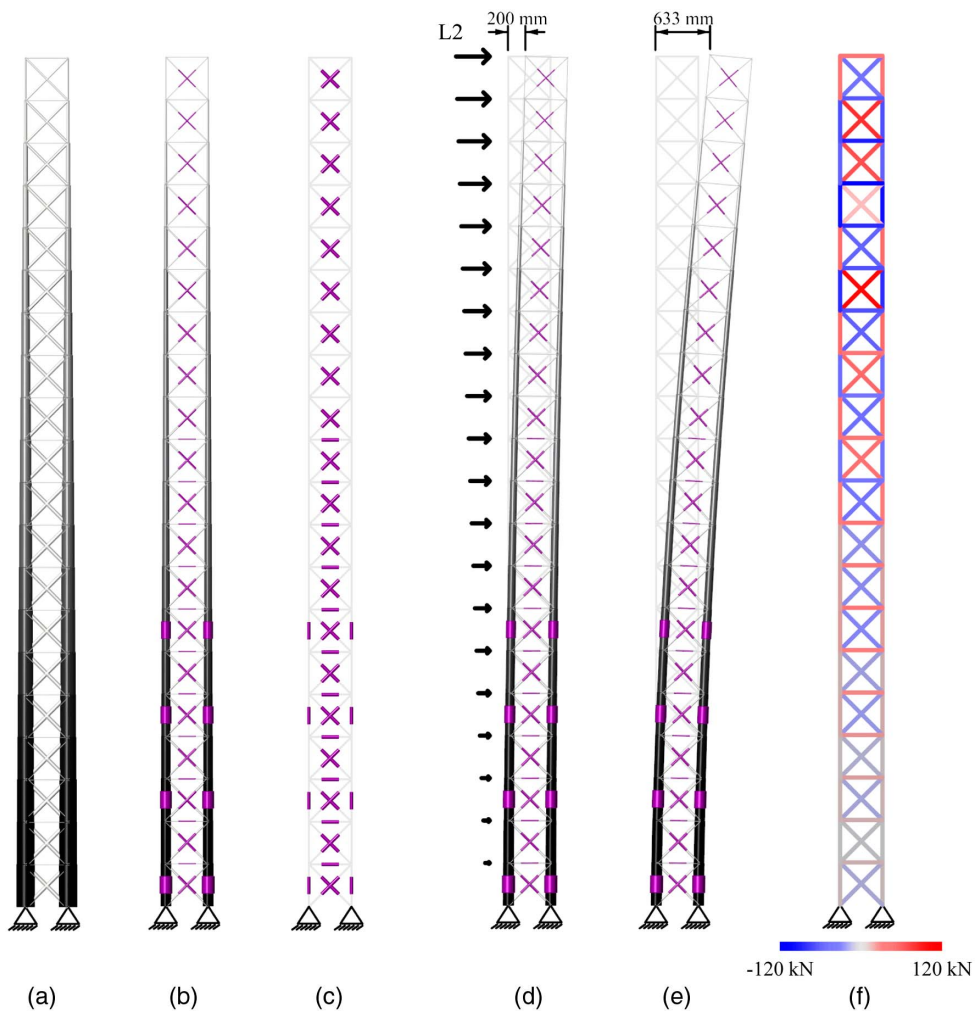

Fig. 7. (a) Passive solution; (b) adaptive solution; (c) actuator layout; (d) controlled shape; (e) deformed shape; and (f) load path redirection under LC2 (magnification ×10; scale 1:800).

displacement compensation and the noncontrolled shape under L2. Without shape change, the tip deflection is 633 mm, which is well beyond the serviceability limit (height/500 = 200 mm). Under live load, the maximum length change is a 4-mm shortening in the bottommost horizontal actuator. The two bottommost vertical actuators apply the greatest tensile (2,200 kN) and compressive (14,000 kN) forces, respectively.

Fig. 7(f) shows the load path redirection, the difference between optimal and compatible internal forces in Load Case L2. For the first half of the truss, the optimal load path is matched via the actuator length changes by adding tension in the horizontal elements and compression in the diagonal bracers. A tension–compression pattern alternates in the second half of the truss where actuators are located exclusively on the diagonals.

Downloaded from ascelibrary.org by University College London on 06/20/18. Copyright ASCE. For personal use only; all rights reserved.

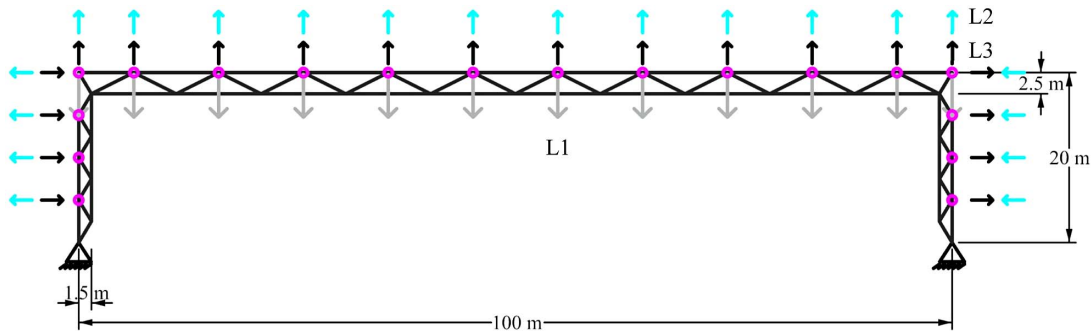

Fig. 8. Portal frame dimensions, loads, and controlled nodes (indicated by circles).

This case study confirms that, for stiffness-governed problems, total energy savings are significant even when the live load has a magnitude substantially lower than that of the dead load (L:D = 0.2). Because civil structures are often designed for low-level L:D ratios, this case study is representative of a large class of real systems. In terms of monetary costs, the passive solution is 16% cheaper with respect to the adaptive one. The control system and maintenance cost shares amount to 42 and 27% of the total cost, respectively. The cost of saving energy using structural adaptation is 0.09 \$/kWh, which is cheaper than the cost of producing energy using PVs (0.13 \$/kWh). Although the adaptive structure is more expensive, it not only uses much lower whole-life energy than the passive structure but is also a competitive solution if thought of as an energy-saving technology.

Portal Frame

The structure considered in this case study is made of planar-trussed portal frames, each supporting 10 m of cover which can represent sections of a typical hangar building. This configuration is investigated here because it is stiffness-governed and is commonly trussed in practice.

Fig. 8 shows one of the portal frames: a 100-m span and a 20-m-tall trussed frame constrained as indicated in the diagram. The vertical displacements of all nodes of the top chord are limited to horizontal span/500, and the total building drift is limited to height/500 (control nodes are indicated by circles in Fig. 8). Because there are 27 CDOFs and the structure is one-time externally statically indeterminate, the minimum number of actuators to control exactly all selected displacements is 27, as discussed in the section "Control System Integration."

The dead load is set to 3 $\mathrm{kN/m^2}$ on the roof panel, resulting in a UDL of 30 kN/m. Three load cases are considered: one is self-weight + dead load; the other two are uniformly distributed loads in opposite directions representing a wind-type load. The live-load maximum intensity is set to 1.5 $\mathrm{kN/m^2}$ (0.5 L:D). Wind pressure is applied on the roof and the cladding panels (both out of plane), supported by the horizontal and vertical trusses, respectively. Table 2 summarizes all load combinations:

Because both loads and geometry are symmetric, the activation threshold is found at 0.75 $\mathrm{kN/m^2}$ for both load cases. In terms of wind velocity, it corresponds to approximately 35 m/s. The total time during which actuation is required to compensate for displacements is 2.8 years (over 50 years).

Fig. 9(a) shows the embodied, operational, and total energy as the MUT varies; the optimal adaptive configuration is found for a MUT of 76%. The passive structure corresponds to a MUT of 38%. In terms of mass and total energy savings, the adaptive structure

Table 2. Portal frame: load combination cases

Case	Load factor	Permanent load	Load factor	Live load
LC1	1.35	L1 = dead load + self-weight	1.5	N/A
LC2 and LC3	0.9	L1 = dead load + self-weight	1.5	L2 and L3 = 1.5 $\mathrm{kN/m^2}$

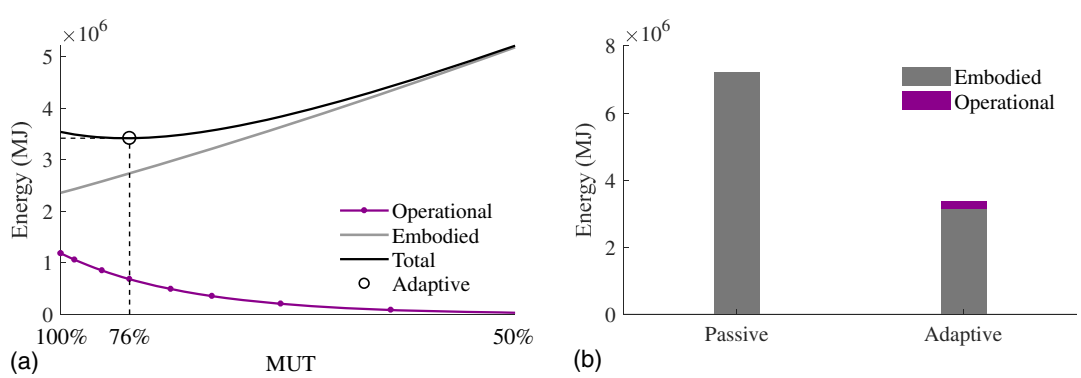

Fig. 9. (a) Embodied, operational, and total energy versus MUT; and (b) passive versus adaptive total energy.

Downloaded from ascelibrary.org by University College London on 06/20/18. Copyright ASCE. For personal use only; all rights reserved.

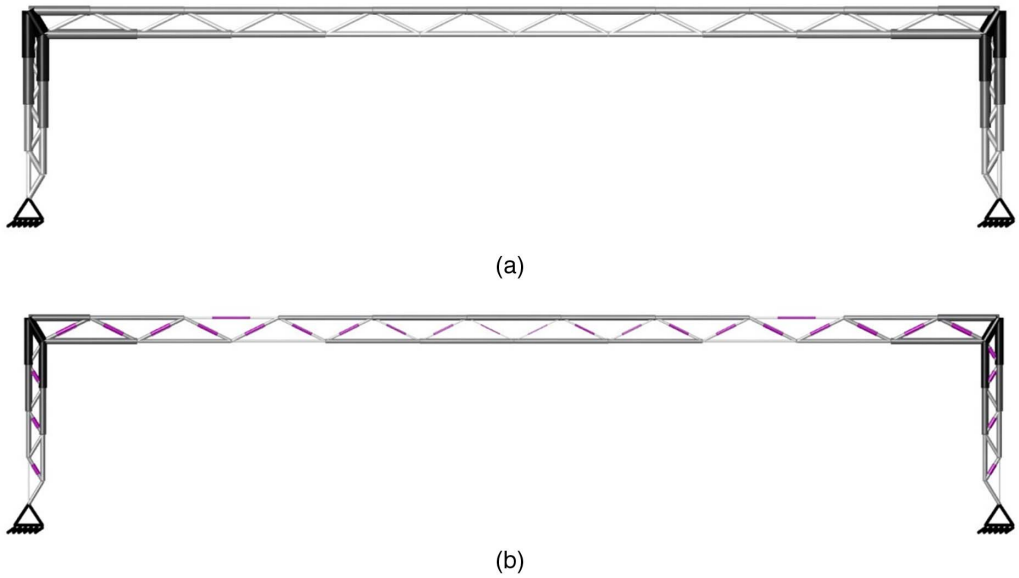

Fig. 10. (a) Passive solution; and (b) adaptive solution (scale 1:800).

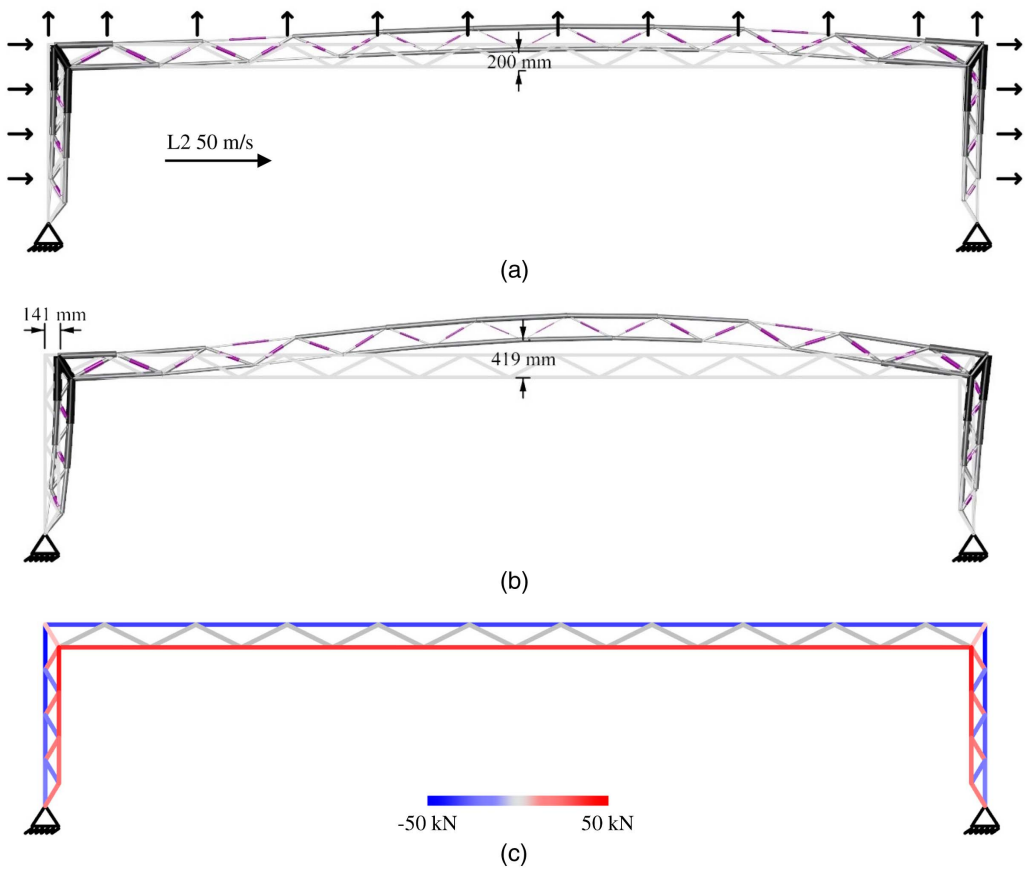

Fig. 11. (a) Controlled shape; (b) deformed shape; and (c) load path redirection under LC2 (magnification ×10; scale 1:900).

achieves 57 and 53%, respectively, compared with the passive structure [Fig. 9(b)]. Fig. 10 compares the optimized passive structure with the adaptive structure. Regarding the adaptive solution, the biggest- and smallest-diameter tubes are 1,700 and 142 mm for, respectively, the outermost diagonal bracers and those at midspan. For the passive solution, these values are more than double. Fig. 11 shows the controlled shape after displacement compensation and the noncontrolled shape under L2. Without shape change, the midspan deflection is 419 mm, which is well beyond the serviceability limit (span/500 = 200 mm). Under live load, the maximum length change is a 9-mm shortening of the diagonal actuators at quarter-length of the horizontal span.

Downloaded from ascelibrary.org by University College London on 06/20/18. Copyright ASCE. For personal use only; all rights reserved.

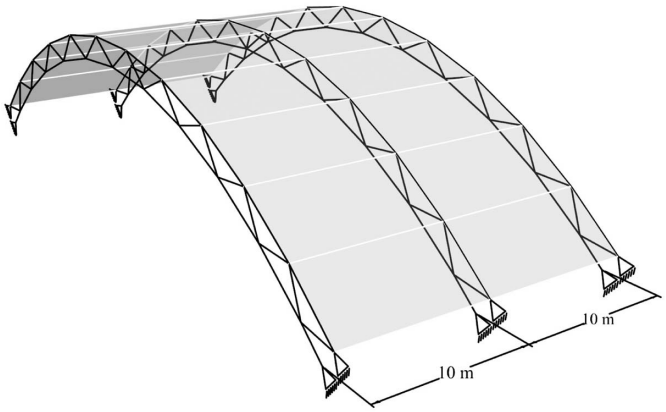

Fig. 12. Catenary arch bridge.

The two bottommost diagonal actuators on the vertical trusses and the two outermost diagonal actuators on the horizontal truss apply the greatest tensile and compressive forces, respectively—approximately 2,300 kN. In terms of load path redirection, the shape change required in this case results mainly in compressive forces in the top chords and tension forces in the bottom chords as shown in Fig. 11(c).

This case study further confirms that, for stiffness-governed designs (as is the case here due to the long span on the portals), energy savings are significant. Little operational energy is needed in this case because the live loads act mainly in the direction opposite to that of the dead load. When the live load is applied, most of the elements of the horizontal part of the structure experience reduced tensile and compressive stresses. During activation, most of the actuators in tension need to extend and, conversely, those in compression must contract. In such situations, there is a theoretical release (or gain) of operational energy. The operational energy for these cases is set to zero.

In monetary terms, the passive solution is 10% cheaper than the adaptive solution. The control system and maintenance amount to 35 and 26% of the total cost respectively. However, the cost of saving energy using structural adaptation in this case is 0.03 \$/kWh, which is cheaper than the cost of producing energy using PVs (0.13 \$/kWh). Therefore, as in the previous case study, although the adaptive solution is more expensive, it uses much lower whole-life energy than the passive solution and is competitive costwise if thought of as an energy-saving technology.

Catenary Arch Bridge

The structure considered in this case study is made of planar trusses that can represent sections of a trussed arch bridge. This configuration is investigated because, unlike the previous case studies, the primary actions are a mix of compression and bending. Each internal truss is assumed to support 10 m of cover as shown in Fig. 12. Fig. 13 shows one of the trusses: a 100-m-span catenary truss arch whose supports are all pinned. Deflection limits are set to span/1,000, which is a value typically used for road bridges with both vehicular and pedestrian traffic (Barker et al. 2011). The vertical displacements of all unconstrained nodes of the top chord are set as CDOFs. Controlled nodes are indicated by circles in Fig. 13. Because there are 10 CDOFs and the static indeterminacy is 3, the minimum number of actuators to control exactly all required displacements is 13, as discussed in the section "Control System Integration."

The dead load is set to 10 kN/m^2 (L1) resulting in a UDL of 100 kN/m. Eight load cases are considered and summarized in Table 3. One is self-weight + dead load. Loads L2–L6 represent a moving load sequence whose magnitude is set to 20 kN/m^2 (L:D of 2). Loads L7 and L8 are two patch loads, each covering one-half of the bridge (e.g., vehicular traffic or train holding). The characteristic load is set to the 95th percentile for the moving load (L2–L6) and 99th percentile for the patch loads (L7 and L8) because they normally occur less frequently than normal traffic. Table 3 summarizes all load case combinations.

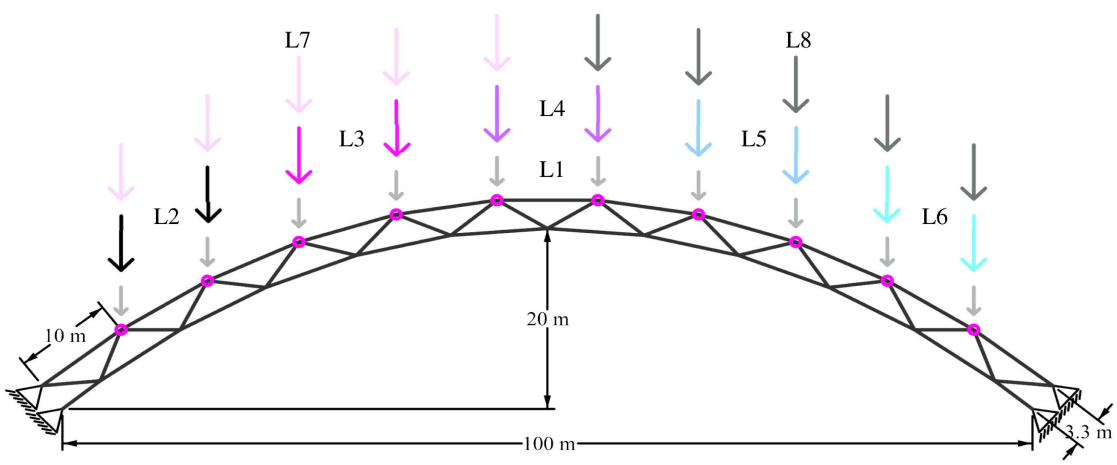

Fig. 13. Catenary arch bridge dimensions, loads, and controlled nodes (indicated by circles).

Table 3. Catenary arch bridge: load combination cases

Case	Load factor	Permanent load	Load factor	Live load	Characteristic load
LC1	1.35	L1 = dead load + self-weight	1.5	N/A	N/A
LC2–LC6	1.35	L1 = dead load + self-weight	1.5	L2–L6 = 20 kN/m^2	95%
LC7 and LC8	1.35	L1 = dead load + self-weight	1.5	L7 and L8 = 20 kN/m^2	99%

J. Struct. Eng., 2018, 144(8): 04018107

Downloaded from ascelibrary.org by University College London on 06/20/18. Copyright ASCE. For personal use only; all rights reserved.

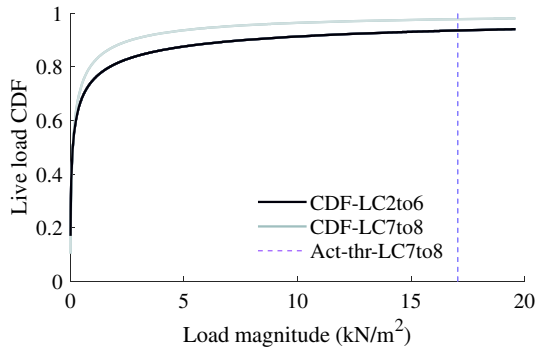

Fig. 14. Live-load CDFs and load activation threshold.

Fig. 14 shows the live-load CDFs for all load cases and the activation thresholds (vertical dashed lines). The activation threshold for load combinations LC2–LC6 is zero because there is never any need to compensate for deflections in these cases. Load Cases LC7 and LC8 have identical activation thresholds because the loads are symmetric. The total time during which actuation is required to compensate for deflections is approximately 2 months (over 50 years).

Fig. 15(a) shows the embodied, operational, and total energy as the MUT varies. The optimal adaptive configuration is found for a MUT of 80%; the passive solution corresponds to a MUT of 71%.

Compared with the passive solution, the adaptive solution saves 18% of the mass and 6% of the total energy [Fig. 15(b)]. Fig. 16 compares the optimized passive structure with the adaptive structure. The biggest- and smallest-diameter tubes for the adaptive solution are 1,200 and 280 mm for the two bottom chord elements closest to the supports and the diagonal bracers at quarter-span, respectively. The passive solution has different element cross sections, the diameter of the bottom chord elements at midspan being 30% larger than in the adaptive solution. Under L8 the maximum length change is 15-mm expansion by the only actuator placed on the opposite side of the top chord shown in Fig. 16(b).

In terms of material efficiency, the ideal load path in an arch bridge is one where the members are in compression even under asymmetric loads. For a trussed arch bridge, this means top and bottom chords should be in compression. This stress state is obtained here by imposing additional constraints to limit element forces to compression. The optimal load path in LC8 is shown in Fig. 17(a). The greatest compressive force is 13,055 kN applied by the actuator placed on the same side of the top chord to which the load is applied. The greatest tensile force is 3,200 kN applied by the diagonal actuator closest to the left pin support. All elements of the top and bottom chords are in compression even under an asymmetric load such as L8, whose magnitude is twice that of the permanent load. Fig. 17(b) shows the load path redirection to achieve this optimal stress state.

Both mass and energy savings are lower than those in the previous case studies mainly due to the shape of the catenary arch structure, which is already very efficient at withstanding downward loads. That having been said, it is worth recalling that displacements are thought of as caused by the live load only, as discussed in the section "Comparison: Adaptive versus Passive." In other

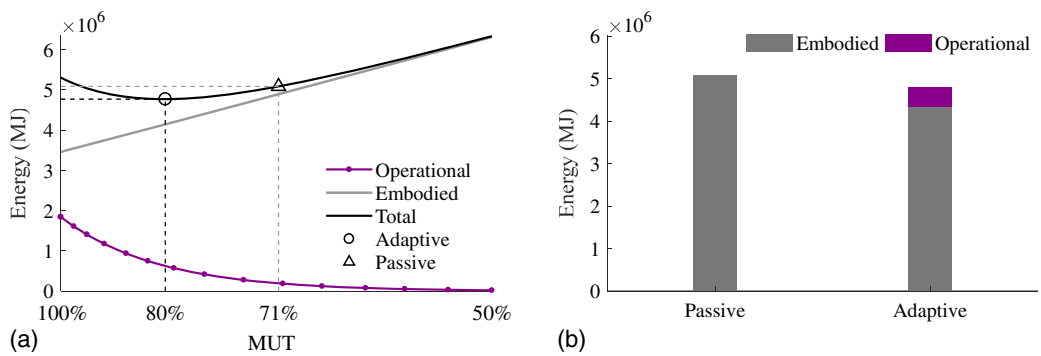

Fig. 15. (a) Embodied, operational, and total energy versus MUT; and (b) passive versus adaptive total energy.

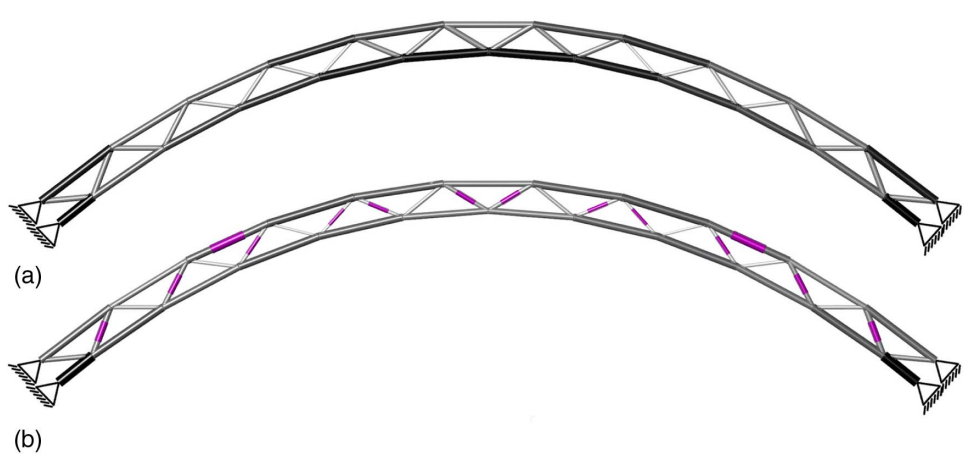

Fig. 16. (a) Passive solution; and (b) adaptive solution (scale 1:800).

Downloaded from ascelibrary.org by University College London on 06/20/18. Copyright ASCE. For personal use only; all rights reserved.

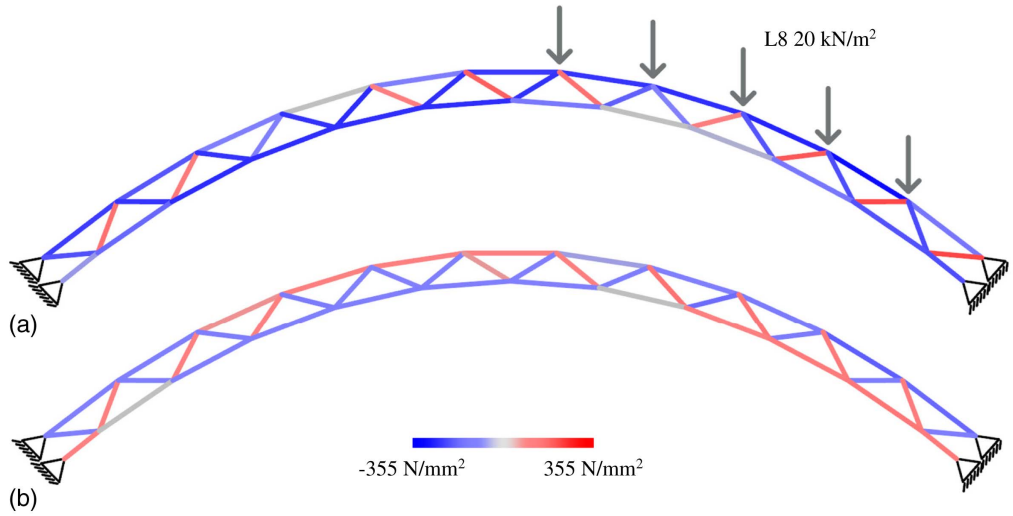

Fig. 17. (a) Optimal load path; and (b) load path redirection under LC8 (scale 1:800).

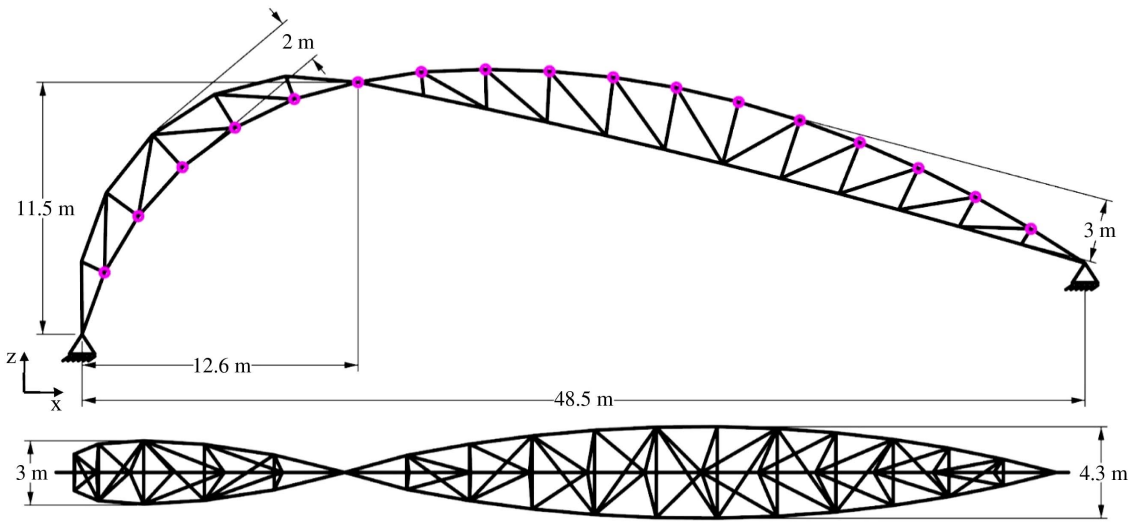

Fig. 18. 3-pin arch dimensions and controlled nodes (indicated by circles).

words, the passive structure is assumed to be perfectly precambered under permanent load, which in this case results in almost no actuation being necessary for displacement compensation. The problem is strength-governed. This also reflects the monetary cost of the passive solution, which is 38% cheaper than the adaptive solution, with control system and maintenance respectively accounting for 26 and 20% of the total cost. The cost of saving energy using adaptation in this case is 0.7 \$/kWh, which is higher than the cost of producing energy using PVs (0.13 \$/kWh).

Roof Arch

The structure considered in this case study is a model of one of the roof arches of London Waterloo Station's former International Terminal. This configuration is selected because it applies to a real-world structure and departs from the previous case studies in that it cannot be reduced to a planar frame.

The roof of the station is supported by a series of 3-pin arches, each made by two dissimilar curved space trusses. Fig. 18 shows one of these roof arches, which has a 50-m span and a rise of 11.5 m. The out-of-plane depth of the shorter truss reaches a maximum of 3 m whereas that of the longer branch reaches 4.3 m (Fig. 18). Although the geometry of the model is close to that of the actual structure, the load cases considered in this study are for illustrative purposes only.

Because the cladding is made of glass, the serviceability limit for vertical and horizontal deflection is set to the horizontal span/500. The vertical displacements of all unconstrained nodes on the long side of the arch are controlled (22 CDOFs). In addition, the horizontal and the vertical displacements of all unconstrained nodes on the short side are controlled for a total of 34 CODFs. The choice of these CDOFs is motivated by the cladding being fixed to the corresponding nodes which are indicated by circles in Fig. 18. The structure is statically determinate, so the minimum number of actuators to control exactly all selected displacements is 34, as discussed in the section "Control System Integration."

Because this is a lightweight structure, the dead load is set to 2 $\mathrm{kN/m^2}$ on the roof panel, and each bay of the truss supports an out-of-plane 10-m-wide span, resulting in a UDL of 20 $\mathrm{kN/m}$. Four load cases are considered: one is self-weight + dead load

Downloaded from ascelibrary.org by University College London on 06/20/18. Copyright ASCE. For personal use only; all rights reserved.

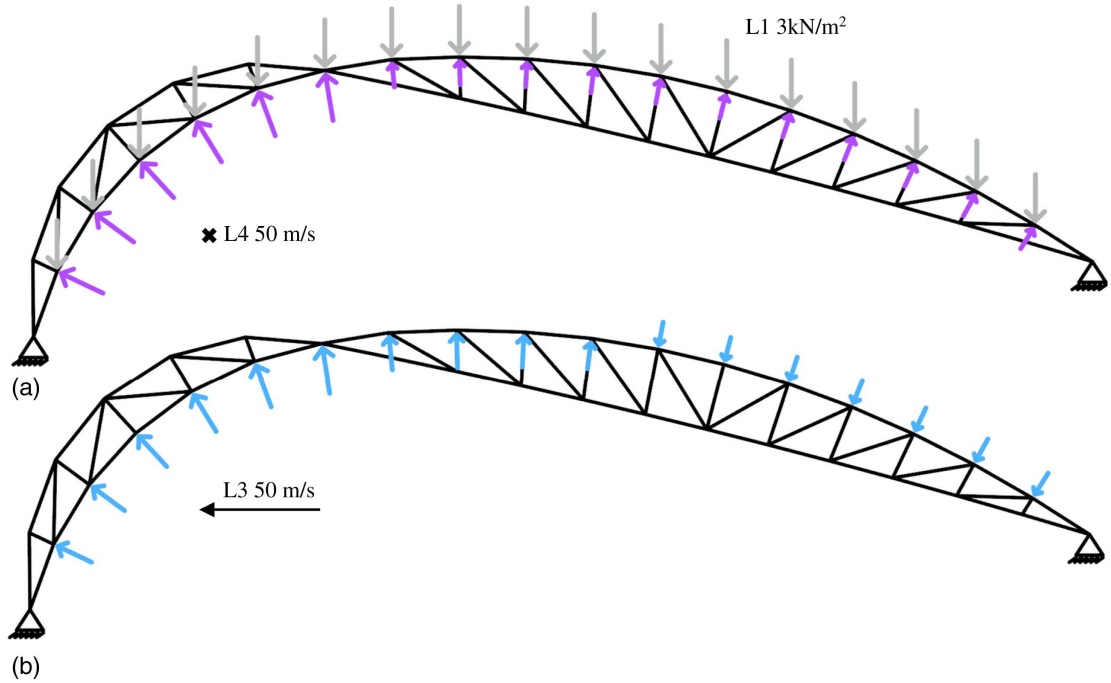

Fig. 19. (a) Dead load L1 and L4 (out-of-plane wind direction); and (b) L3.

Table 4. 3-pin trussed arch geometry: load combination cases

Case	Load factor	Permanent load	Load factor	Live load
LC1	1.35	L1 = dead load + self-weight	1.5	N/A
LC2–LC4	0.9	L1 = dead load + self-weight	1.5	L2–L4 = 1.5 kN/m^2

and the other three are wind-type loads, two of which (L2 and L3) have opposite directions in the plane as shown in Fig. 19(b) (L2 not represented), and one of which (L4) is orthogonal to the plane as shown in Fig. 19(a) (upward arrows). The live-load maximum intensity is set to 1.5 kN/m^2 (L:D of 0.75). Wind pressure is applied on the roof panes and tributary loads derived at the nodes. Pressure coefficients for each pane are determined by the angle between the wind direction and the normal to the pane as described in Eurocode 1 (CEN 1991). All load combinations are summarized in Table 4.

The live-load cumulative distributions are identical for all load cases. The activation threshold for LC3 is found at zero because, for this load case, there is no need for actuation to compensate for deflections. When the wind is directed toward the long side of the truss (L3), the pressure coefficients are lower than those for L2 or L4 because the shape of this side is more aerodynamically efficient. The respective activation thresholds for LC2 and LC4 are 0.72 and 0.84 kN/m^2. In terms of wind velocity, the lowest load activation threshold (LC2) corresponds to approximately 34 m/s. The total time during which actuation is required to compensate for deflections is approximately 12 months for L2 and 9 months for L4.

Fig. 20(a) shows the embodied, operational, and total energy as the MUT varies. The optimal adaptive configuration is found for a MUT of 100%. The elements of the adaptive structure work at

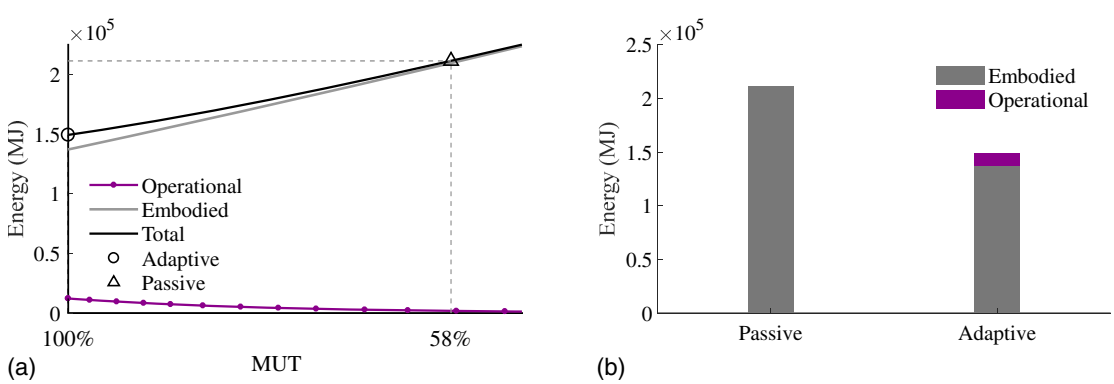

Fig. 20. (a) Embodied, operational, and total energy versus MUT; and (b) passive versus adaptive total energy.

Downloaded from ascelibrary.org by University College London on 06/20/18. Copyright ASCE. For personal use only; all rights reserved.

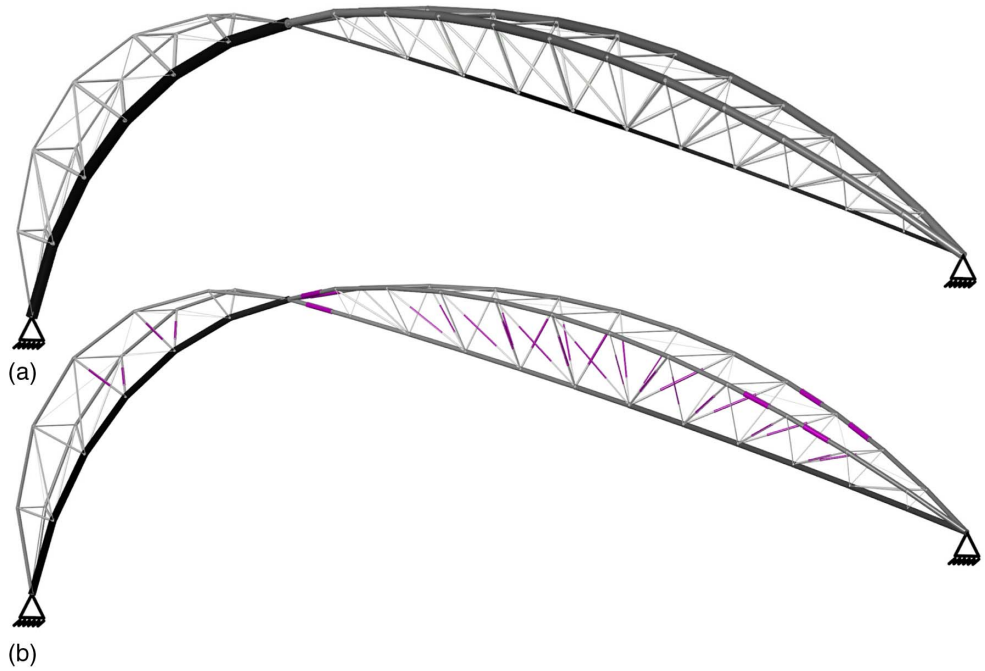

Fig. 21. (a) Passive solution; and (b) adaptive solution. Perspective view.

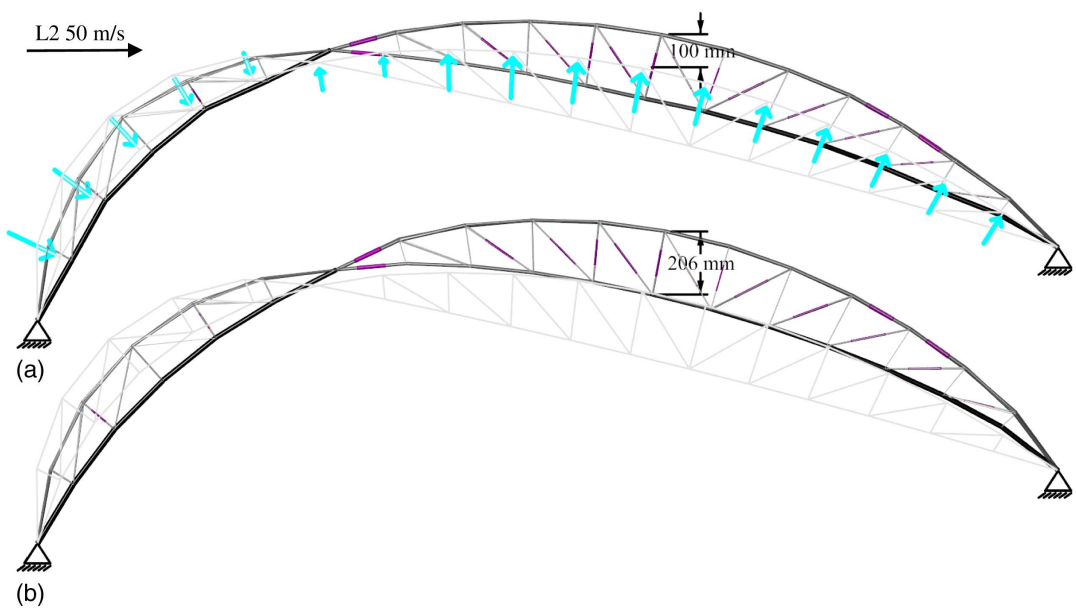

Fig. 22. (a) Controlled shape and (b) deformed shape under L2 (magnification ×15; scale 1:400).

capacity (100% used) for the worst case (L1—permanent load only) whereas deflections above serviceability limits are dealt with by the active system. The passive structure corresponds to a MUT of 58%. The adaptive structure achieves 35 and 29% of mass and total energy savings, respectively, compared with the passive structure as shown by the bar chart in Fig. 20(b). As with the portal frame case study, little operational energy is needed because the live load acts mainly opposite to the dead load. During deployment, most of the actuators in tension need to extend and, conversely, those in compression must contract. In both cases, there is a theoretical release or gain of operational energy. The operational energy for these cases is set to zero.

Fig. 21 compares the optimized passive structure with the adaptive structure. The biggest- and smallest-diameter members for the adaptive solution are respectively 244 and 12 mm for the bottom chord elements closest to the supports and the diagonal bracers of the top chord. Fig. 22 shows the controlled shape after displacement compensation and the noncontrolled shape under L2. Without shape change, the maximum deflection is 206 mm, which is beyond the serviceability limit (span/500 = 100 mm). Under L2 the maximum length change is a 27-mm expansion by the bottom chord actuator closest to the central pin. The greatest compressive force is 180 kN applied by the top chord actuators closest to the right-side support pin. The greatest tensile forces are approximately 20 kN

Downloaded from ascelibrary.org by University College London on 06/20/18. Copyright ASCE. For personal use only; all rights reserved.

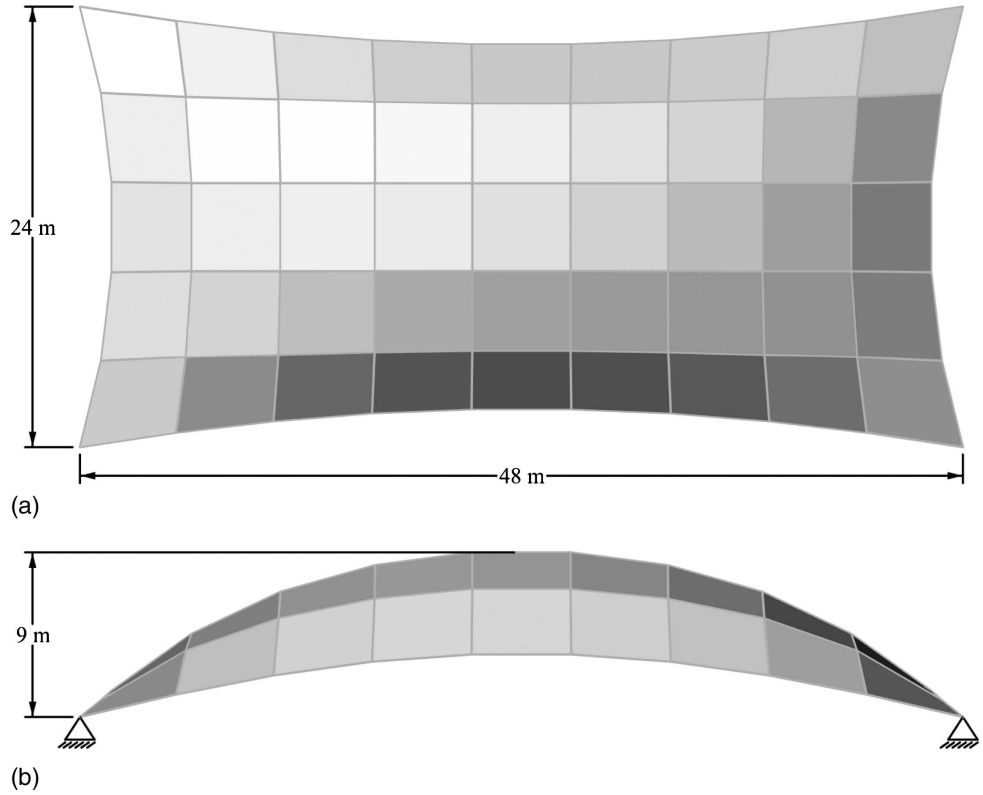

Fig. 23. Double-curved shell: (a) top view; and (b) elevation.

applied by the actuators placed on the diagonal bracers between the top and bottom chords on the short-side arch truss. In this case there is no load path redirection because the structure is statically determinate and therefore actuator length changes do not affect the stresses (for small displacements) (Senatore et al. 2013).

The model considered in this case study confirms that, even for complex spatial structures, the adaptive solution outperforms the passive solution in terms of whole-life energy consumption. However, in terms of monetary costs, in this case the passive solution is 95% cheaper than the adaptive solution and the cost of saving energy via actuation is 10.9 $/kWh, which is much higher than the cost of producing energy using PVs (0.13 $/kWh). In contrast to the first two case studies, due to layout complexity and small material usage, this configuration has a very high control system density (defined in the section "Control System Integration"): 144 sensors and 34 actuators distributed in approximately 0.4 m^3 (see also Table 7). This results in control system and maintenance being, respectively, 56 and 41% of the total cost. To reduce control system cost, displacement compensation can be achieved using fewer actuators albeit with lower accuracy. In addition, because the control forces are relatively low (on the order of 100 kN), actuation technologies that do not require expensive power distribution systems like those required by hydraulic actuators may be considered (section "Monetary Cost").

Double-Curved Shell

Fig. 23 shows a synclastic grid shell whose form was generated using a shape optimization routine based on dynamic relaxation (Day 1965; Barnes 1977; Wakefield 1980; Williams 2000; Senatore and Piker 2015). This configuration is selected to investigate the effectiveness of the adaptive solution when applied to an already efficient 3D load-bearing system.

The input geometry is a flat rectangular mesh. The quadrangular face edges connect the structural nodes acting as tension/compression elements. The element cross sections and their stiffness are set to a low value to make the structure flexible. Element masses and rotational inertia are lumped at nodes. The corner nodes are pinned. Gravity load is applied.

The reticular structure, shown in Fig. 24, is built using the optimized mesh geometry just described. It consists of three layers: the bottom layer [Fig. 24(a)] is a quadrangular pattern that hosts the external cladding; the middle layer [Fig. 24(b)] consist of elements that start from the vertices of the quadrangles in Fig. 24(a) and meet along the normal from their center at 0.5 m (depth); the top layer [Fig. 24(c)] is the dual of the quadrangular pattern. All displacements (x, y, z) of the nodes that connect directly to the cladding (Layer a) are limited to span/500. Control nodes are indicated by dots in Fig. 24(a). Because there are 93 CDOFs and the degree of static indeterminacy is 27, 120 actuators in total are needed to control exactly all selected displacements (see the section "Control System Integration").

Five load cases are considered: one is self-weight + dead load and the other four are wind-type loads arranged in two pairs with opposite directions (Fig. 25). Because this is a lightweight structure, the dead load is set to 2 kN/m^2 on the roof panel. The intensity of the live load varies quadratically with the height, reaching a maximum of 1.5 kN/m^2 (L:D of 0.75). Both dead load and wind pressure are applied on the roof panes and tributary loads are derived at the nodes. Pressure coefficients are determined by the angle between the wind direction and the normal to the pane as described in Eurocode 1 (CEN 1991). All load combinations are described in Table 5.

Fig. 26 shows the live-load cumulative distribution functions for all load cases that have identical probability distribution. The vertical dashed lines represent the activation thresholds.

Downloaded from ascelibrary.org by University College London on 06/20/18. Copyright ASCE. For personal use only; all rights reserved.

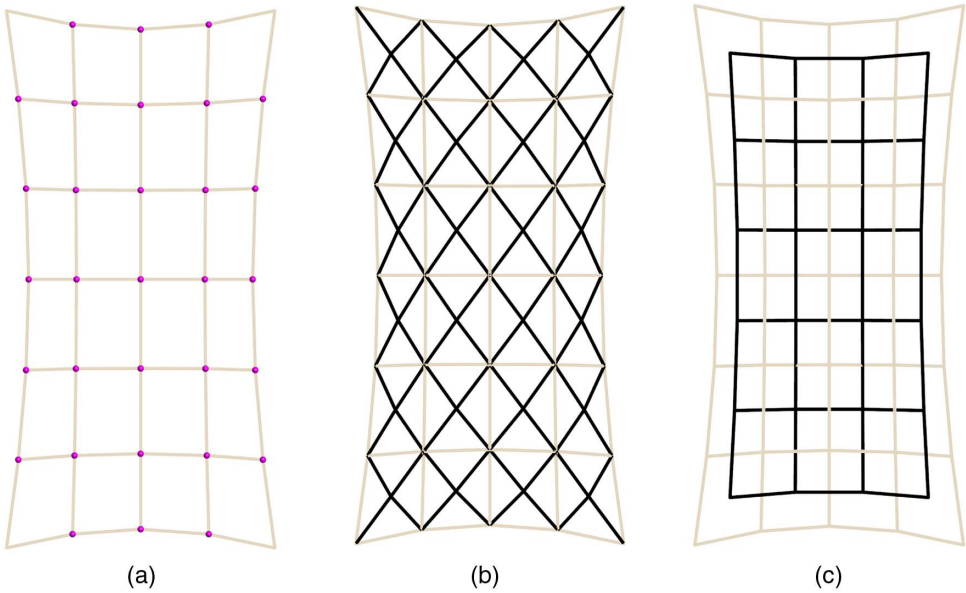

Fig. 24. (a) Top layer and controlled nodes (indicated by dots); (b) middle layer; and (c) bottom layer.

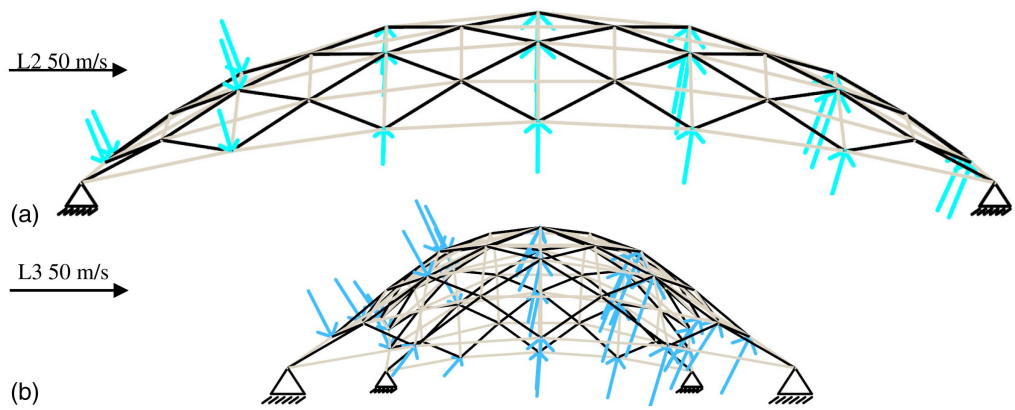

Fig. 25. (a) L2 (opposite L4); and (b) L3 (opposite L5).

Table 5. Synclastic curved shell: load combination cases

Case	Load factor	Permanent load	Load factor	Live load
LC1	1.35	L1 = dead load + self-weight	1.5	N/A
LC2–LC5 5	0.9	L1 = dead load + self-weight	1.5	L2–L5 = 1.5 kN/m^2

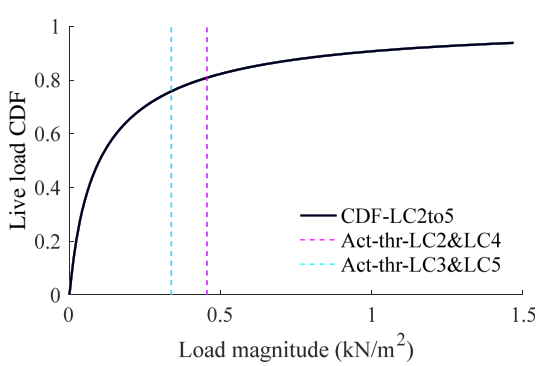

Fig. 26. Live-load CDFs and load activation threshold.

Due to the biaxial symmetry of the structure and applied loads, the activation thresholds are pairwise identical: LC2 and LC4 and LC3 and LC5. The activation threshold for LC2–LC4 is lower than that for LC3–LC5 because, when the wind is orthogonal to the main span, larger displacements compared with the other case are the result. In terms of wind velocity, the lowest load activation threshold (LC3 or LC5) corresponds to approximately 23 m/s. The total time during which actuation is required to compensate for deflection is 8 years (over 50 years)—approximately 3.3 years for LC2 or LC4 and approximately 4.7 years for LC3 or LC5.

Fig. 27(a) shows the embodied, operational, and total energy as the MUT varies. The optimal adaptive configuration is found for a MUT of 38%; the passive structure corresponds to a MUT of 27%.

Downloaded from ascelibrary.org by University College London on 06/20/18. Copyright ASCE. For personal use only; all rights reserved.

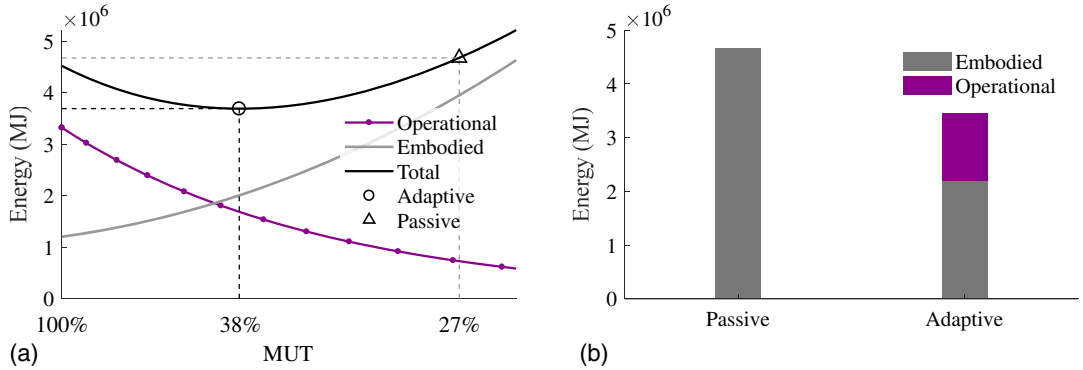

Fig. 27. (a) Embodied, operational, and total energy versus MUT; and (b) passive versus adaptive total energy.

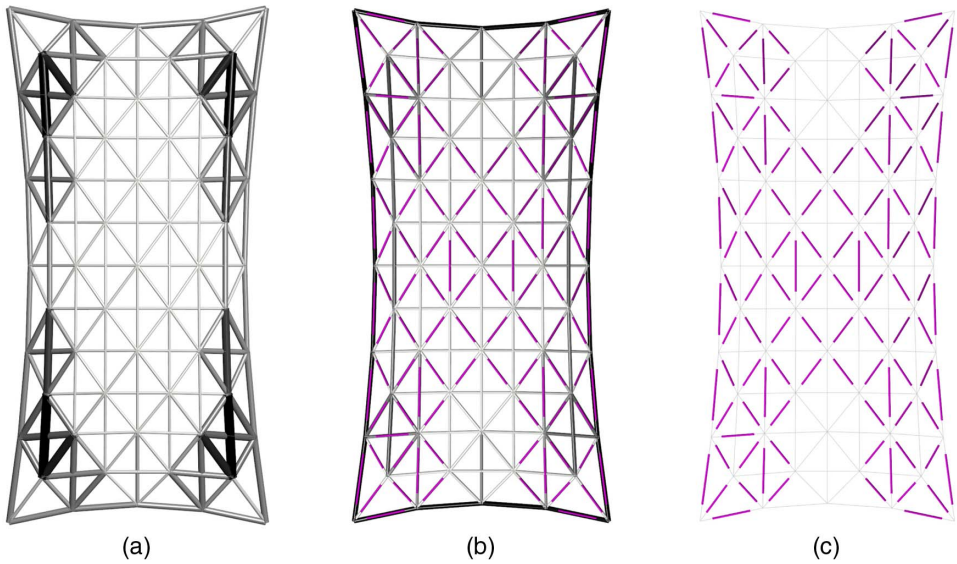

Fig. 28. (a) Passive solution; (b) adaptive solution; and (c) actuator layout (scale 1:600).

In terms of mass and total energy savings, the adaptive structure achieves 52 and 26%, respectively, compared with the passive structure, as shown by the bar chart in Fig. 27(b).

Fig. 28 compares the optimized passive structure with the adaptive structure. The biggest- and smallest-diameter members for the adaptive solution are 600 and 320 mm for one of the edge elements and the top-layer elements, respectively [Fig. 24(c)]. Fig. 28(c) shows the actuator positions represented on the bare layout. The actuators are located mostly on the edge elements of the bottom layer and on the diagonal elements of the middle layer. Fig. 29 shows the difference between the controlled and noncontrolled shape for L2. Without active displacement compensation, the maximum deflection is 340 mm, which is beyond the serviceability limit (span/500 = 100 mm). Under L2 the maximum length changes are approximately 6-mm expansion by the actuators on the edge elements closest to the right pin support (Fig. 29). The greatest compressive forces are approximately 1,500 kN applied by the actuators placed on the edges of the short side. The greatest tensile forces are approximately 900 kN applied by some of the diagonal actuators. The load path redirection for LC2 is shown in Fig. 30. The shape change in this case requires adding compressive forces by the actuators in the edge elements and in most of the diagonal elements.

Being generated by form finding, the shape efficiently resists the permanent load without much bending; however, the wind loading produces large displacements, making the problem stiffness-governed. As with previous examples, in these cases force redirection and displacement compensation via actuation significantly outperform purely passive resistance to loads. In terms of monetary costs, the passive solution is 66% cheaper than the adaptive one and the cost of saving energy via actuation is 0.91 \$/kWh, which is higher than the cost of producing energy using PVs (0.13 \$/kWh). This configuration has a high control system density: 56 sensors and 18 actuators per cubic meter. This which makes the control system and maintenance dominant (86%) with respect to material cost. In this case, because all nodes of the bottom layer [Fig. 24(a)] are controlled in all directions, several actuators (120 in total) are needed for displacement compensation and force redirection. To reduce control system cost, fewer nodes should be selected and lower control accuracy should be considered via the use of fewer actuators than the minimum number defined in the section "Control System Integration." In addition, because control forces for this case do not exceed 500 kN, other actuation technology may be considered that does not require expensive power distribution systems such as the case of hydraulics, as discussed in the section "Monetary Cost."

Downloaded from ascelibrary.org by University College London on 06/20/18. Copyright ASCE. For personal use only; all rights reserved.

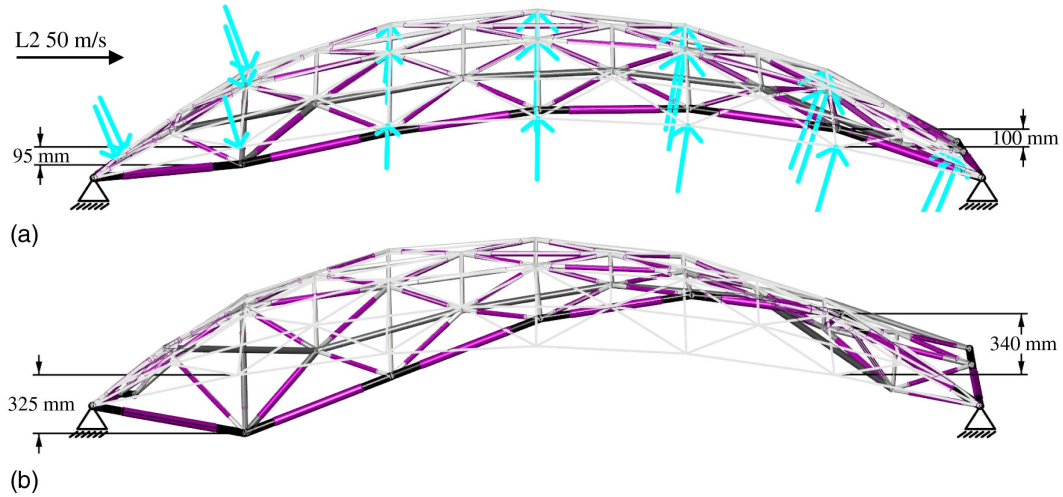

Fig. 29. (a) Controlled shape and (b) deformed shape under L2 (magnification ×10; scale 1:400).

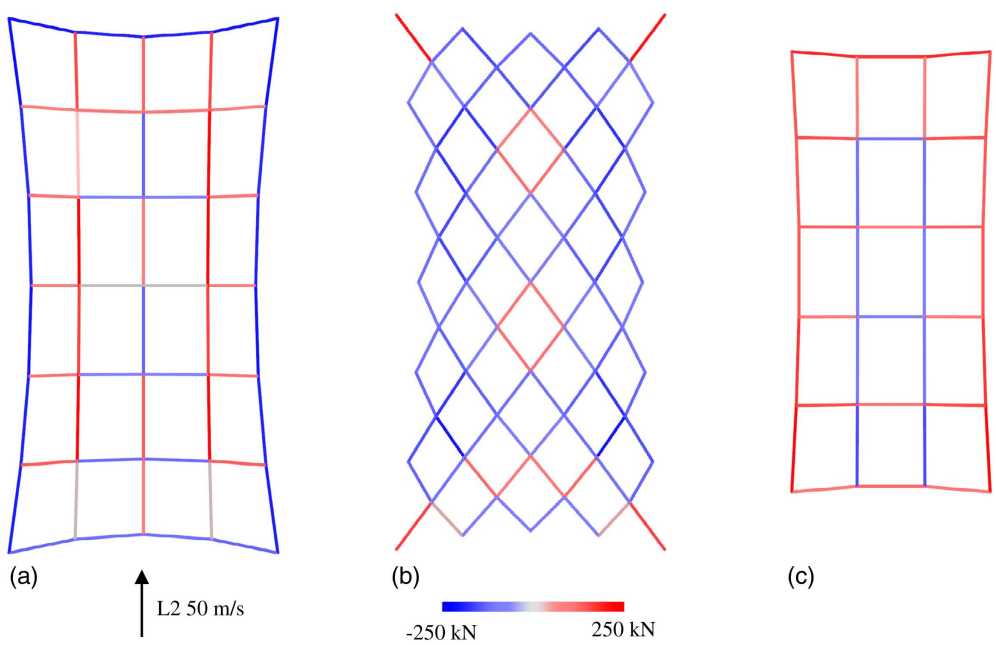

Fig. 30. Load path redirection under LC2: (a) bottom layer; (b) middle layer; and (c) top layer.

Exoskeleton Tower

The structure considered in this final case study is a simplified model of a tower building at 30 St Mary Axe, informally known as the Gherkin. This is a tall building in the City of London. The model is loosely related to the original geometry, which is studied here as a possible example of a tall building resisting external loads through an exoskeleton structure. This means that, in this case study, the building is assumed to have no structural core (although the real Gherkin does). Because cores significantly reduce commercially usable floor space, systems that can do away with them free up their floor layouts and are therefore of structural, architectural, and commercial interest.

The main aim of this case study is to investigate how energy savings and cost differences between the adaptive and passive configuration vary with the slenderness (i.e., H:D ratio) for a complex 3D layout. Two models are considered, the first having a H:D ratio of 3 with a height of 180 m and a depth of 60 m (the biggest floor depth), the second having a H:D ratio of 5 with a height of 300 m. The radial and vertical element spacing (i.e., mesh aspect ratio) is identical for both models. Figs. 31(a and b) show the elevation view for the two configurations. Supports (all pins) are applied to the nodes as indicated in the diagrams.

The total building drift is set to height/500 (Griffis 1993). Control nodes are indicated by dots in Figs. 31(a and b). The horizontal displacements of all nodes but the supports are controlled for a total of 194 and 322 CDOFs when the H:D ratios are, respectively, 3 and 5. The degree of static indeterminacy is 5, so 199 and 327 actuators are needed to control exactly the selected displacements (section "Control System Integration") for the former

Downloaded from ascelibrary.org by University College London on 06/20/18. Copyright ASCE. For personal use only; all rights reserved.

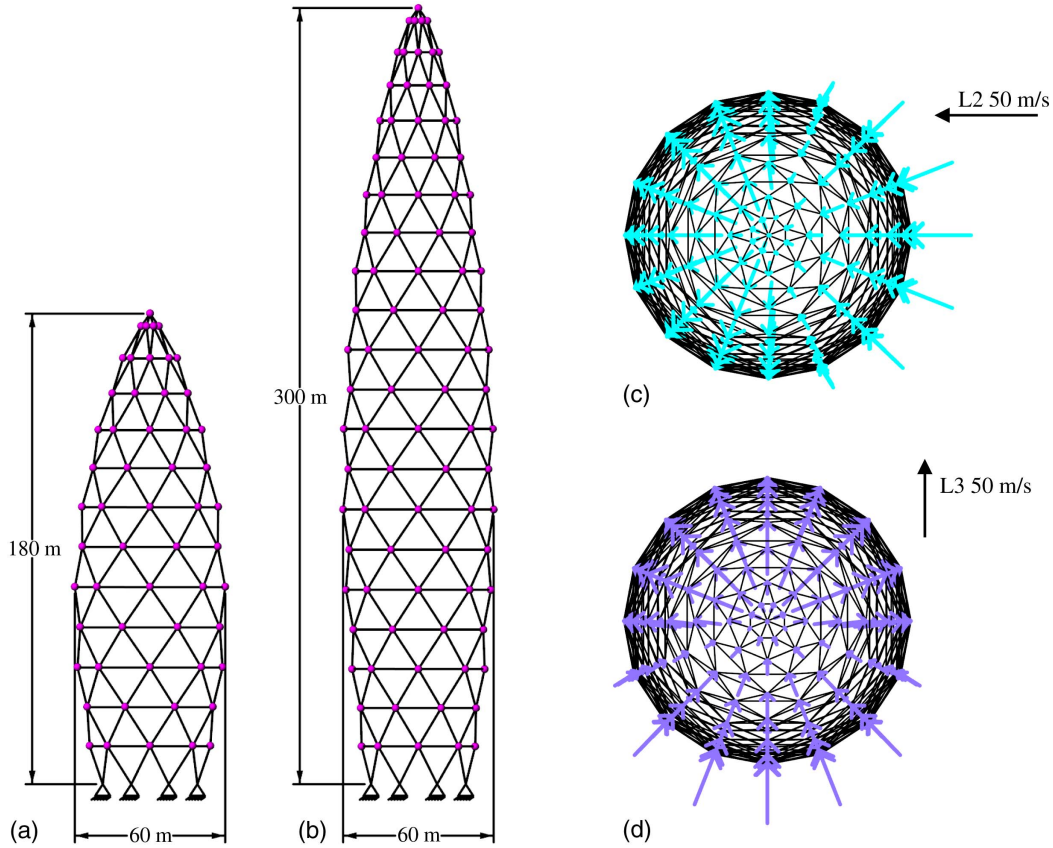

Fig. 31. Dimensions and control nodes (indicated by dots): (a) H:D = 3; (b) H:D = 5; (c) L2; and (d) L3.

Table 6. Exoskeleton tower: load combination cases

Case	Load factor	Permanent load	Load factor	Live load
LC1	1.35	L1 = dead load + self-weight	1.5	N/A
LC2–LC5	1.35	L1 = dead load + self-weight	1.5	L2–L5 = 1.5 kN/m^2

and the latter, respectively. Because the total number of actuators is very high, making the control system extremely complex, it is reduced to 50 and 200 for the model with respective H:D ratios of 3 and 5. Using fewer actuators than those required to control exactly the selected DOFs results in displacement residuals. The reduced actuator numbers are obtained ensuring that controlled displacements still stay within serviceability limits at the expense of extra operational energy.

Five load cases are considered. Load L1 is self-weight + dead load, which is set to 3 kN/m^2 on the floors of the building and transmitted on the nodes of the exoskeleton structure. The live load consists of four wind-type load cases arranged in two pairs with opposite directions. Fig. 31(c) is a top view of the structure with L2 (symmetrical to L4); Fig. 31(d) shows L3 (symmetrical to L5) applied. The live-load intensity varies quadratically with the height, reaching a maximum of 1.5 kN/m^2 (L:D of 0.5). Both dead load and wind pressure are applied to the roof panes, and tributary loads are derived at the nodes. Pressure coefficients for each pane are determined by the angle between the wind direction and the normal to the pane as described in Eurocode 1 (CEN 1991). Load combination cases are summarized in Table 6.

All live-load cases have identical probability distribution. The activation thresholds are 1.0 and 0.7 kN/m^2 for respective H:D ratios of 3 and 5. For each structure, the activation thresholds are identical for all load cases because of symmetry. In terms of wind velocity, they correspond to approximately 40 and 34 m/s. The total time during which actuation is required to compensate for deflections is 1.25 and 3 years.

Fig. 32(a) shows the embodied, operational, and total energy as the MUT varies for both cases. Mass and total energy savings compared with those for the passive structure are 25 and 8% for H:D = 3 and 48 and 31% for H:D = 5 [bar chart in Fig. 32(b)]. The optimal adaptive structure is found for a MUT of 51% for the former and 43% for the latter. This is because, for a higher H:D, displacement compensation takes more operational energy and therefore must be minimized by decreasing the MUT. The passive structure corresponds to a MUT of 42% for the former and 24% for the latter.

Fig. 33 compares the optimized passive structure with the adaptive structure for H:D = 3. The biggest- and smallest-diameter tubes for the adaptive solution are 2,200 and 154 mm for the bottommost and topmost elements, respectively. For the passive solution, the maximum diameter is quite similar (2,260 mm); however, the minimum diameter is almost double that of the adaptive solution. The actuators are located mostly toward the bottom of the structure because that is where they are most effective in reducing larger displacements of the top nodes.

Downloaded from ascelibrary.org by University College London on 06/20/18. Copyright ASCE. For personal use only; all rights reserved.

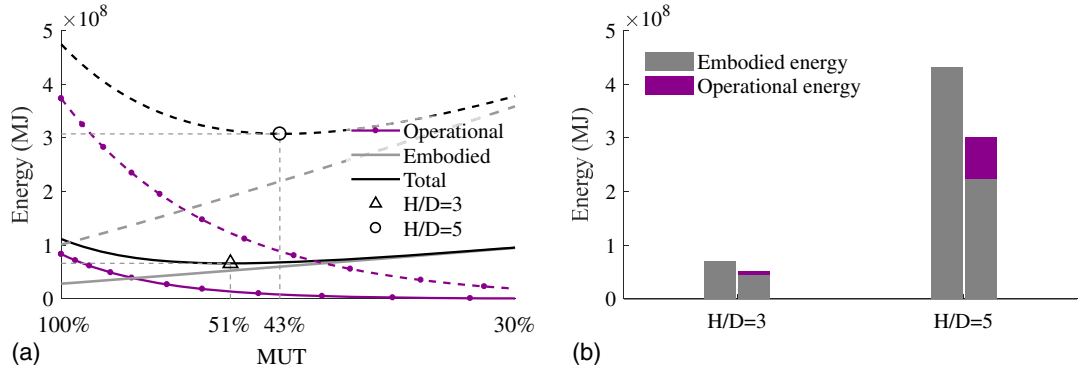

Fig. 32. (a) Embodied, operational, and total energy versus MUT; and (b) passive versus adaptive total energy.

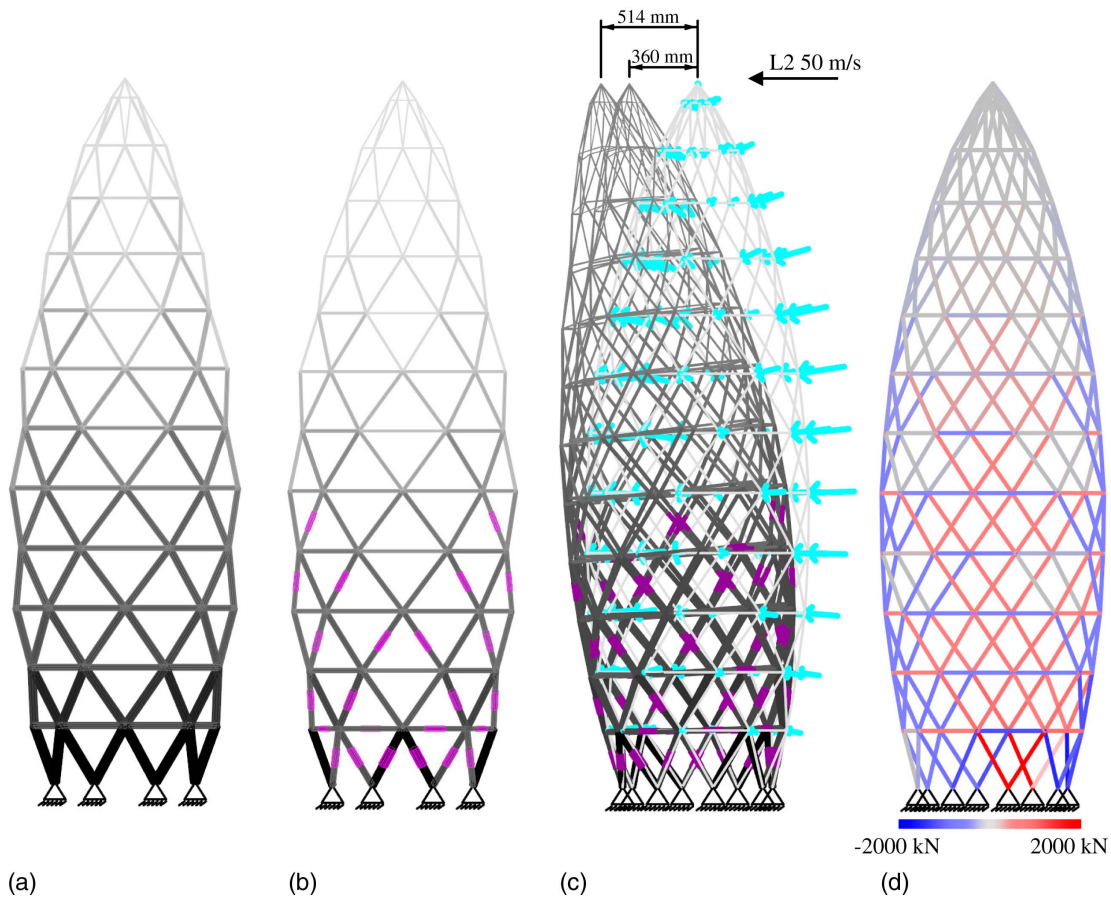

Fig. 33. (a) Passive configuration; (b) adaptive configuration; (c) controlled and deformed shape; and (d) load path redirection under LC2 (magnification ×50; scale 1:2, 000).

Fig. 33(c) shows the difference between controlled and noncontrolled displacements under L2. Without active displacement compensation, the max deflection is 514 mm, which is beyond the serviceability limit (height/500 = 360 mm). Under L2 the max length change is an approximate 25-mm expansion made by the bottommost actuators located on the side opposite to the side on which the load is applied, which must deploy under the greatest compressive forces (14,500 kN). The greatest tensile forces are approximately 7,000 kN applied by the actuators placed on the horizontal elements (which can be thought of as tightening "rings" on a basket-like structure). The load path redirection for LC2 is illustrated in Fig. 33(d). Matching the optimal load path requires adding compressive forces on the side where the wind load hits the structure and on the opposite side, which is subjected to negative pressure. Tensile forces are required in the orthogonal direction to the lateral load.

Similar analysis can be carried out for the more slender case, which is shown in Fig. 34. The biggest- and smallest-diameter tubes for the adaptive solution are 3,300 and 130 mm for the bottommost and topmost elements, respectively. For the passive solution, maximum and minimum diameters are 4,500 and 1,200 mm, respectively. Without active displacement compensation, the maximum

Downloaded from ascelibrary.org by University College London on 06/20/18. Copyright ASCE. For personal use only; all rights reserved.

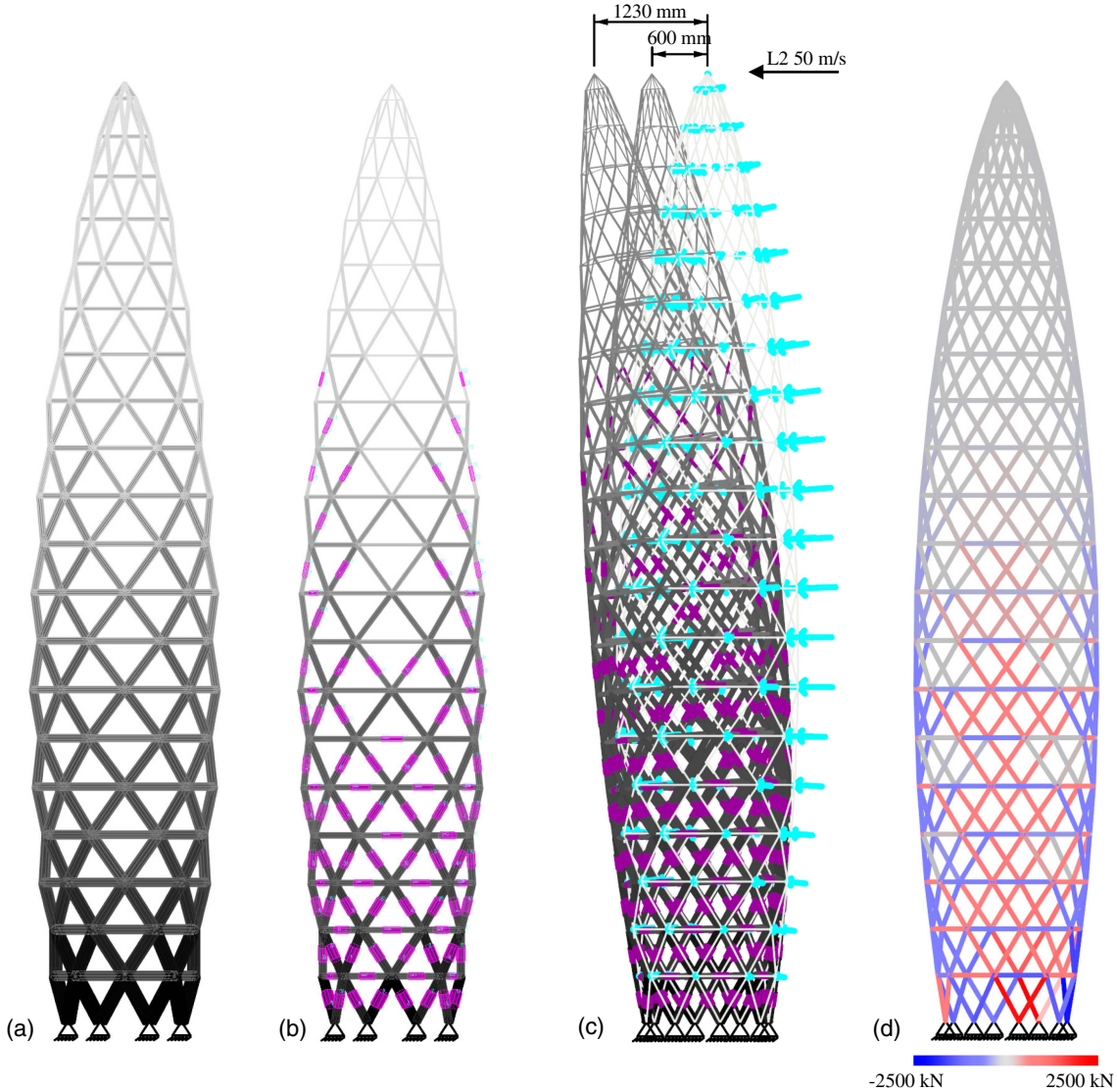

Fig. 34. (a) Passive configuration; (b) adaptive configuration; (c) controlled and deformed shape; and (d) load path redirection under LC2 (magnification ×50; scale 1:2, 000).

deflection is 1,230 mm, which is beyond the serviceability limit (height/500 = 600 mm). Under L2 the maximum length changes are an approximate 40-mm expansion made by the bottommost actuators as per H:D = 3, which must deploy under the greatest compressive forces (35,000 kN). The greatest tensile forces are approximately 18,000 kN applied by the actuators placed on the horizontal elements as in the H:D = 3 case.

Regarding monetary costs for the case of H:D = 3, the passive solution is 24% cheaper than the adaptive one and the cost of energy saving via actuation is 0.22 \$/kWh, which is comparable to the cost of producing energy using PVs (0.13 \$/kWh). This configuration has a low density of 11 sensors and 0.5 actuators per cubic meter, with a control system and maintenance combined cost of 44%. However, mass savings and energy savings are relatively low and thus do not compensate for the control system cost penalty. In contrast, for H:D = 5 the passive solution is 30% more expensive than the adaptive one. Control system density is less for H:D = 3, having 4.5 sensors and 0.3 actuators per cubic meter and substantial mass and energy savings (48 and 30%). Because in this case monetary savings derive from the passive solution, saving energy via actuation produces a gain of 0.1 \$/kWh compared with the cost of producing energy using PV systems.

This case study shows that, for buildings supported by an exoskeleton (i.e., no core), even with a low ratio of height to depth (in this case 1:3) total energy savings can be achieved. As expected, the savings become substantial when slenderness (H:D ratio) increases. For both cases, although the number of actuators and sensors is high, control system density is low because of the amount of material mass used by the structure. Low sensor and actuator density, combined with substantial mass and energy savings, make the adaptive solution a competitive one in monetary terms.

Discussion

From the case studies investigated in this paper, it is now possible to assess quantitatively the benefits of adaptive designs. Table 7 provides a summary of results for all case studies. The table shows performance metrics for more stringent serviceability criteria as well. For all cases, when serviceability limits are halved, energy savings increase by at least 15% and can reach 60%.

J. Struct. Eng., 2018, 144(8): 04018107

Downloaded from ascelibrary.org by University College London on 06/20/18. Copyright ASCE. For personal use only; all rights reserved.

Table 7. Performance metrics summary

Serviceability limit state	Mass savings (%)	Energy savings (%)	L:D ratio	MUT (%)	Activation time (years)	CS density (nSens|nActs)/m^3	CS cost (%)	Cost ($) penalty (%)	Cost ($) (kWh)
Multistory building core									
SLS = height/500	62	42	0.5	45	5.3	(20|5)	69	16	0.04
SLS = height/1,000	79	63	0.5	41	9.6	(19|5)	67	−63	−0.06
Portal frame									
SLS = span/360|height/500	57	53	0.5	85	3.6	(17|3)	61	10	0.02
SLS = span/500|height/1,000	72	67	0.5	76	9.3	(17|3)	61	−40	−0.05
Catenary arch bridge									
SLS = span/1,000	18	6	2	83	0.1	(9|1)	46	37	0.5
SLS = span/2,000	31	16	2	52	0.2	(6|0.5)	35	6	0.02
SLS = span/4,000	54	31	2	40	0.6	(4|0.4)	29	−53	−0.08
Roof arch									
SLS = span/500	29	26	0.5	100	1.7	(311|81)	95	95	7.76
SLS = span/2,000	82	72	0.5	100	9.0	(311|81)	95	82	0.7
SLS = span/4,000	88	83	0.5	81	12.1	(233|61)	95	65	0.3
Double-curved shell									
SLS = span/500	57	20	0.75	46	8.0	(56|17)	86	71	0.65
SLS = span/1,000	75	51	0.75	38	14.6	(56|17)	86	46	0.16
SLS = span/2,000	84	72	0.75	31	17.4	(46|14)	84	0.3	0.001
Exoskeleton tower (H:D = 3)									
SLS = height/500	25	8	0.5	51	1.2	(11|0.5)	44	24	0.18
SLS = height/1,000	34	25	0.5	35	2.6	(8|0.3)	36	−14	−0.04
Exoskeleton tower (H:D = 5)									
SLS = height/500	48	30	0.5	43	3.0	(4.5|0.3)	30	−30	−0.07
SLS = height/1,000	70	50	0.5	38	6.2	(4|0.2)	27	−145	−0.11

Note: (nSens|nActs)/m^3 = xly means x sensors and y actuators per cubic meter.

Even structures with shapes optimized against permanent loads, such as the catenary arch bridge and the double-curved dome, achieve energy savings of up to 30 and 50%, respectively.

Even more significant energy savings are achieved when the slenderness of the structure increases, as shown by the exoskeleton case study. Conversely, when defection limits are stricter or the structure is more slender, the MUT decreases because the work required for displacement compensation via actuation increases and involves a higher level of operational energy. In other words, the contribution of the material to limit deflections is comparatively more efficient when serviceability constraints are stricter; hence, the optimum configuration is found for a lower MUT.

A cost analysis was carried out for each case study showing a similar pattern. Under conventional deflection limits, the adaptive solution tends to be more expensive than the passive solution due to control system costs. However, stricter deflection limits make the use of structural adaptation also competitive monetarily. A control system density index was used to appreciate how structural layout complexity relates to monetary cost. When mass savings are substantial and control system density is low, the cost penalty of the adaptive solution is small and eventually becomes a gain for stricter deflection limits. In addition, a benchmark against the cost of conventional energy savings technologies, such as PV systems, shows that for slender structures and low control system density, the cost of saving energy using structural adaptation is competitive.

Deflection limits used for the examples described in this paper are those commonly used by practicing design engineers. These criteria were chosen to reach an overall performance and economic optimum within an old paradigm in which a building structure must withstand external loads by relying only on material strength and stiffness. If the structure is adaptive instead, it takes only a small amount of extra operational energy to control deflections even for very strict limits. More stringent deflection limits could improve structure performance in several ways, including structural integrity, comfort, and risk mitigation for damages to fittings/claddings that can occur when large deformations occur.

Conclusions

This paper provides a performance analysis of several adaptive structure configurations ranging from planar to complex 3D reticular systems. For all configurations studied, the adaptive solution outperformed the corresponding passive optimized version in terms of mass and total energy use. The passive structures were already optimized using state-of-the-art methods. As expected, for strength-governed design problems (e.g., the catenary arch bridge), the energy savings are lower. For stiffness-governed structures instead, the energy savings are substantial because it is challenging to limit deflections solely by adding more material (i.e., the passive solution).

From the results shown in Table 7, it can be inferred that both mass and energy savings generally increase apace with stricter serviceability limits. The same trend applies to the control system cost penalty, which becomes small for stiffness-governed structures. Using stricter deflection limits shows that the use of structural adaptation can also be competitive in monetary terms. For adaptive solutions that achieve both substantial mass and energy savings and low sensor and actuator densities, the cost of saving energy using adaptation competes with that of conventional energy-saving technologies. Even when monetary costs do not favor an adaptive design, there may be other considerations that make it appealing such as extreme slenderness and increased floor space.

Acknowledgments

The authors gratefully acknowledge the Engineering and Physical Sciences Research Council (EPSRC) for providing core funding for

Downloaded from ascelibrary.org by University College London on 06/20/18. Copyright ASCE. For personal use only; all rights reserved.

this project through the University College London (UCL) Doctoral Training Centre in Urban Sustainability and Resilience (Grant No. EP/G037698/1). Also acknowledged is Expedition Engineering, the project industrial partner that provided significant additional resources. The EPFL Applied Computing and Mechanics Laboratory (IMAC) is thankfully acknowledged for its support during the review process of this article.

References

Abdel-Rohman, M., and H. Leipholz. 1983. "Active control of tall buildings." *J. Struct. Eng.* 109 (3): 628–645.

Adam, B., and I. F. Smith. 2008. "Active tensegrity: A control framework for an adaptive civil-engineering structure." *Comput. Struct.* 86 (23–24): 2215–2223. https://doi.org/10.1016/j.compstruc.2008.05.006.

Barker, G. M., J. Staebler, and K. Barth. 2011. *Serviceability limits and economical steel bridge design*. Rep. No. FHWA-HIF-11-044. Washington, DC: US Dept. of Transportation.

Barnes, M. R. 1977. "Form finding and analysis of tension space structures by dynamic relaxation." Ph.D. dissertation, City Univ. London.

Begg, D., and X. Liu. 2000. "On simultaneous optimization of smart structures. II: Algorithms and examples." *Comput. Methods Appl. Mech. Eng.* 184 (1): 25–37.

Campanile, L. F. 2005. "Initial thoughts on weight penalty effects in shape-adaptable systems." *J. Intelligent Mater. Syst. Struct.* 16 (1): 47–56. https://doi.org/10.1177/1045389X05046692.

CEN (European Committee for Standardization). 1991. *Actions on structures: General actions. Part 1-4: Wind*. Eurocode 1, Brussels.

Cha, J., J. Pitarresi, and T. Soong. 1988. "Optimal design procedures for active structures." *J. Struct. Eng.* 114 (12): 2710–2723. https://doi.org/10.1061/(ASCE)0733-9445(1988)114:12(2710).

Day, A. 1965. "An introduction to dynamic relaxation." *Engineer* 219: 218–221.

ENERPAC. 2016. "E328e industrial tools: Europe." Accessed July 12, 2017. http://www.enerpac.com/en-us/downloads.

Fest, E., K. Shea, B. Domer, and F. Smith. 2003. "Adjustable tensegrity structures." *J. Struct. Eng.* 129 (4): 515–526. https://doi.org/10.1061/(ASCE)0733-9445(2003)129:4(515).

Griffis, L. G. 1993. "Serviceability limit states under wind load." *Eng. J. Am. Inst. Steel Construct.* 30 (1): 1–16.

Hammond, G., and C. Jones. 2008. *Inventory of carbon & energy (ICE)*. Univ. of Bath, Bath, UK.

Hasse, A., and L. F. Campanile. 2009. "Design of compliant mechanisms with selective compliance." *Smart Mater. Struct.* 18 (11): 115016. https://doi.org/10.1088/0964-1726/18/11/115016.

Henry, A., C. W. Karm, C. Lewis, M. Smith, M. King, R. Wong, S. Munro, S. L. Ming, N. Boulter, and P. A. Howd. 2016. "Singapore sports hub: Engineering the National Stadium." *Struct. Eng.* 94 (9): 26–37.

Huber, J. E., N. A. Fleck, and M. F. Ashby. 1997. "The selection of mechanical actuators based on performance indices." *Proc. R. Soc. A* 453 (1965): 2185–2205. https://doi.org/10.1098/rspa.1997.0117.

Jenkins, C. 2005. *Compliant structures in nature and engineering*. 1st ed. Southampton, UK: WIT Press.

Khot, N. 1998. "Multicriteria optimization for design of structures with active control." *J. Aerosp. Eng.* 11 (2): 45–51. https://doi.org/10.1061/(ASCE)0893-1321(1998)11:2(45).

Korkmaz, S. 2011. "A review of active structural control: Challenges for engineering informatics." *Comput. Struct.* 89 (23–24): 2113–2132. https://doi.org/10.1016/j.compstruc.2011.07.010.

Lu, L. Y., S. Uktu, and B. Wada. 1992. "On the placement of active members in adaptive truss structures for vibration control." *Smart Mater. Struct.* 1 (1): 8–23. https://doi.org/10.1088/0964-1726/1/1/003.

Neuhäuser, S. 2014. "Untersuchungen zur Homogenisierung von Spannungsfeldern bei adaptiven Schalentragwerken mittels Auflagerverschiebung." Ph.D. dissertation, Univ. of Stuttgart.

Nowak, A. S., and K. R. Collins. 2012. *Reliability of structures*. 2nd ed. Boca Raton, FL: Taylor & Francis.

NREL (National Renewable Energy Laboratory). 2012. "A performance calculator for grid-connected PV systems." Accessed April 2, 2012. http://rredc.nrel.gov/solar/calculators/PVWATTS/version1/.

Onoda, J., and R. Haftka. 1987. "An approach to structure/control simultaneous optimization for large flexible spacecraft." *AIAA J.* 25 (8): 1133–1138. https://doi.org/10.2514/3.9754.

Patnaik, S., A. Gendy, S. Berke, and D. Hopkins. 1998. "Modified fully utilized design (MFUD) method for stress and displacement constraints." *Int. J. Numer. Methods Eng.* 41 (7): 1171–1194. https://doi.org/10.1002/(SICI)1097-0207(19980415)41:7<1171::AID-NME296>3.0.CO;2-O.

Preumont, A., B. de Marneffe, A. Deraemaeker, and F. Bossensb. 2008. "The damping of a truss structure with a piezoelectric transducer." *Comput. Struct.* 86 (3–5): 227–239. https://doi.org/10.1016/j.compstruc.2007.01.038.

Reinhorn, A. S. T., R. Lin, and M. Riley. 1992. *Active bracing system: A full scale implementation of active control*. Rep. NCEER-92-0020. Buffalo, NY: National Center for Earthquake Engineering Research.

Rodellar, J., V. Mañosa, and C. Monroy. 2002. "An active tendon control scheme for cable-stayed bridges with model uncertainties and seismic excitation." *Struct. Contr. Health Monit.* 9 (1): 75–94. https://doi.org/10.1002/stc.4.

Schnellenbach, M. H., and D. Steiner. 2014. "Self-tuning closed-loop fuzzy logic control algorithm for adaptive prestressed structures." *Struct. Eng. Int.* 24 (2): 163–172. https://doi.org/10.2749/101686614X13830790993528.

SCX (Street Crane Xpress). 2010. "Wimbledon Centre Court Retractable Roof." Accessed September 15, 2016. http://www.scxspecialprojects.co.uk/cache/filelibrary/73/library/fileLibrary/2011/6/Wimbledon.pdf.

Senatore, G., P. Duffour, S. Hanna, P. Winslow, and C. Wise. 2013. "Designing adaptive structures for whole life energy savings." In *Proc., Fifth Int. Conf. on Structural Engineering, Mechanics and Computation*, 2105–2110. London, UK: Taylor & Francis.

Senatore, G., P. Duffour, P. Winslow, and C. Wise. 2018. "Shape control and whole-life energy assessment of an 'infinitely stiff' prototype adaptive structure." *Smart Mater. Struct.* 27 (1): 015022. https://doi.org/10.1088/1361-665X/aa8cb8.

Senatore, G., and D. Piker. 2015. "Interactive real-time physics: An intuitive approach to form-finding and structural analysis for design and education." *Comput. Aided Des.* 61: 32–41. https://doi.org/10.1016/j.cad.2014.02.007.

Sobek, W. 1987. "Auf pneumatisch gestützten Schalungen hergestellte Betonschalen." Ph.D. dissertation, Univ. of Stuttgart.

Sobek, W., and P. Teuffel. 2001. "Adaptive systems in architecture and structural engineering." In Vol. 4330 of *Proc., Smart Structures and Materials 2001: Smart Systems for Bridges, Structures, and Highways*. 36–46. Bellingham, WA: International Society for Optics and Photonics.

Soong, T. T. 1988. "State of the art review: Active structural control in civil engineering." *Eng. Struct.* 10 (2): 74–84. https://doi.org/10.1016/0141-0296(88)90033-8.

Soong, T. T., and J. Chang. 1982. "Active vibration control of large flexible structures." *Shock Vib. Bull.* 52: 47–54.

Soong, T. T., and G. Cimellaro. 2009. "Future directions in structural control." *Struct. Contr. Health Monit.* 16 (1): 7–16. https://doi.org/10.1002/stc.291.

TATA Steel. 2012. "Sections publications." Accessed March 18, 2013. http://www.tatasteeleurope.com/en/products_and_services/products/long/sections/sections_publications/.

Teuffel, P. 2004. "Entwerfen Adaptiver Strukturen." Ph.D. dissertation, Univ. of Stuttgart.

Tibert, G. 2002. "Deployable tensegrity structures for space applications." Ph.D. dissertation, Royal Institute of Technology.

Utku, S. 1998. *Theory of adaptive structures: Incorporating intelligence into engineered products*. Boca Raton, FL: CRC Press.

Vishay. 2015. "Micro-measurements." Accessed December 2015. http://www.vishaypg.com/micro-measurements/.

Downloaded from ascelibrary.org by University College London on 06/20/18. Copyright ASCE. For personal use only; all rights reserved.

Wakefield, D. 1980. "Dynamic relaxation analysis of pre-tensioned networks supported by compression arches." Ph.D. dissertation, City Univ. London.

Weilandt, A. 2007. "Adaptivität bei Flächentragwerken." Ph.D. dissertation, Univ. of Stuttgart.

Williams, C. 2000. "British museum great court roof." Accessed April 14, 2013. http://people.bath.ac.uk/abscjkw/BritishMuseum/.

Xu, B., S. Wu, and K. Yokoyama. 2003. "Neural networks for decentralized control of cable-stayed bridge." *J. Bridge Eng.* 8 (4): 229–236. https://doi.org/10.1061/(ASCE)1084-0702(2003)8:4(229).

Downloaded from ascelibrary.org by University College London on 06/20/18. Copyright ASCE. For personal use only; all rights reserved.